NAVAL POSTGRADUATE SCHOOL

MONTEREY, CALIFORNIA

THESIS

FLEXIBLE MULTIBODY DYNAMICS AND CONTROL OF THE BIFOCAL RELAY MIRROR

by

Brian M. Moore

December 2003

Thesis Advisor:	Brij N. Agrawal
Second Reader:	Marcello Romano

THIS PAGE INTENTIONALLY LEFT BLANK

REPORT DOCUMENTATION PAGE			Form Approved OMB No. 0704-0188
Public reporting burden for this collection of information is estimated to average 1 hour per response, including the time for reviewing instruction, searching existing data sources, gathering and maintaining the data needed, and completing and reviewing the collection of information. Send comments regarding this burden estimate or any other aspect of this collection of information, including suggestions for reducing this burden, to Washington headquarters Services, Directorate for Information Operations and Reports, 1215 Jefferson Davis Highway, Suite 1204, Arlington, VA 22202-4302, and to the Office of Management and Budget, Paperwork Reduction Project (0704-0188) Washington DC 20503.			
1. AGENCY USE ONLY ***(Leave blank)***	**2. REPORT DATE** December 2003	**3. REPORT TYPE AND DATES COVERED** Engineer's and Master's Thesis	
4. TITLE AND SUBTITLE: Flexible Multibody Dynamics and Control of the Bifocal Relay Mirror		**5. FUNDING NUMBERS**	
6. AUTHOR(S) Brian M. Moore			
7. PERFORMING ORGANIZATION NAME(S) AND ADDRESS(ES) Naval Postgraduate School Monterey, CA 93943-5000		**8. PERFORMING ORGANIZATION REPORT NUMBER**	
9. SPONSORING /MONITORING AGENCY NAME(S) AND ADDRESS(ES) N/A		**10. SPONSORING/MONITORING AGENCY REPORT NUMBER**	
11. SUPPLEMENTARY NOTES The views expressed in this thesis are those of the author and do not reflect the official policy or position of the Department of Defense or the U.S. Government.			
12a. DISTRIBUTION / AVAILABILITY STATEMENT **Approved for public release; distribution is unlimited.**		**12b. DISTRIBUTION CODE**	

13. ABSTRACT ***(maximum 200 words)***

In recent years, spacecraft have become increasingly flexible. The design requirements for the Bifocal Relay Mirror spacecraft include controlling jitter at the nanoradian level. Typically, tight pointing requirements require high structural stiffness, at the cost of increasing the on-orbit mass. To accomplish this, while minimizing the mass of the spacecraft, the structure will have some inherent flexibility. These flexible modes will interact with the pointing control, hence affecting the payload performance. The compensator design conducted in this thesis achieves order of magnitude improvements in controlling the rate error, hence jitter. This thesis starts with a rigid body dynamic model, and develops a flexible body dynamic model. Once the model is developed, the structure-controls interaction is discussed. Finally, compensators are applied to the rigid body controller to mitigate the performance losses present in the flexible body system. Through classical second-order compensators, the angular rate error was decreased by a factor of ten. Nonminimum phase notch filters and phase lag filters were used. Ultimately, the phase lag filters provided the best performance.

14. SUBJECT TERMS Controls, Flexible, Flexibility, Structure, Compensator, Filter, Bifocal Relay Mirror, Modal, Modes, Laser, Satellite, Spacecraft, MATLAB, SIMULINK, Attitude	**15. NUMBER OF PAGES** 77
	16. PRICE CODE

17. SECURITY CLASSIFICATION OF REPORT	**18. SECURITY CLASSIFICATION OF THIS PAGE**	**19. SECURITY CLASSIFICATION OF ABSTRACT**	**20. LIMITATION OF ABSTRACT**
Unclassified	Unclassified	Unclassified	UL

NSN 7540-01-280-5500

Standard Form 298 (Rev. 2-89)
Prescribed by ANSI Std. 239-18

THIS PAGE INTENTIONALLY LEFT BLANK

Approved for public release; distribution is unlimited.

FLEXIBLE MULTIBODY DYNAMICS AND CONTROL OF THE BIFOCAL RELAY MIRROR

Brian M. Moore
Captain, United States Army
B.S., Purdue University, 1993
M.S.A., Central Michigan University, 2001

Submitted in partial fulfillment of the
requirements for the degrees of

AERONAUTICAL AND ASTRONAUTICAL ENGINEER
and
MASTER OF SCIENCE IN ASTRONAUTICAL ENGINEERING

from the

NAVAL POSTGRADUATE SCHOOL
December 2003

Author: Brian M. Moore

Approved by: Brij N. Agrawal
Thesis Advisor

Marcello Romano
Second Reader

Anthony J. Healey
Chairman, Department of Mechanical and
Astronautical Engineering

THIS PAGE INTENTIONALLY LEFT BLANK

ABSTRACT

In recent years, spacecraft have become increasingly flexible. The design requirements for the Bifocal Relay Mirror spacecraft include controlling jitter at the nanoradian level. Typically, tight pointing requirements require high structural stiffness, at the cost of increasing the on-orbit mass. To accomplish this, while minimizing the mass of the spacecraft, the structure will have some inherent flexibility. These flexible modes will interact with the pointing control, hence affecting the payload performance. The compensator design conducted in this thesis achieves order of magnitude improvements in controlling the rate error, hence jitter. This thesis starts with a rigid body dynamic model, and develops a flexible body dynamic model. Once the model is developed, the structure-controls interaction is discussed. Finally, compensators are applied to the rigid body controller to mitigate the performance losses present in the flexible body system. Through classical second-order compensators, the angular rate error was decreased by a factor of ten. Nonminimum phase notch filters and phase lag filters were used. Ultimately, the phase lag filters provided the best performance.

THIS PAGE INTENTIONALLY LEFT BLANK

TABLE OF CONTENTS

LIST OF FIGURES

LIST OF EQUATIONS

THIS PAGE INTENTIONALLY LEFT BLANK

ACKNOWLEDGMENTS

I would like to thank my wife, Kristin, and my children, Mickey and Tess. Without their love, support, and companionship, this work would not have been possible. You're what it's all about. Thank you family! I love you whole bunches!

THIS PAGE INTENTIONALLY LEFT BLANK

I. INTRODUCTION

Recently, spacecraft designs have become more flexible in comparison to the legacy satellites, which are more rigid. There are also designs that involve multibody motion, such as a moving payload on a slewing central bus. The Bifocal Relay Mirror combines these situations for the purpose of relaying a laser from a ground or air source to space relay, to a ground or air target or receiver. The target may be cooperative, in the case of optical communications or other non-force application purposes, or uncooperative in the case of high-energy applications.

Increasing the precision of the acquisition, tracking and pointing sequence demands that multibody dynamics and flexible dynamic effects be combined and addressed from a control design perspective. This thesis presents the rigid body and flexible body dynamics, and compares the uncompensated and compensated performance of the spacecraft using a flexible plant. Classical compensator designs are reviewed and applied.

The design requirements for the Bifocal Relay Mirror spacecraft include controlling jitter at the nanoradian level. Typically, tight pointing requirements require high structural stiffness, at the cost of increasing the on-orbit mass. To accomplish this, while minimizing the mass of the spacecraft, the structure will have some inherent flexibility. These flexible modes will interact with the pointing control, hence affecting the payload performance. The compensator design conducted in this thesis achieves order of magnitude improvements in controlling the rate error, hence jitter.

Through classical second-order compensators, the angular rate error was decreased by a factor of ten. Nonminimum phase notch filters and phase lag filters were used. Ultimately, the phase lag filters yielded the best performance.

THIS PAGE INTENTIONALLY LEFT BLANK

II. BIFOCAL RELAY MIRROR RIGID BODY EQUATIONS OF MOTION

This section presents the derivations from Appendix B of the Bifocal Relay Mirror Technology Development paper submitted by the Naval Postgraduate School in February 2002 for the National Reconnaissance Office Directors Innovation Initiative competition. It provides the derivations of the equations of motion for the bifocal relay mirror spacecraft. The spacecraft sketch and relative size are shown in Figure 1. It consists of two bodies, transmit telescope and receive telescope. The receive telescope rotates with respect to the transmit telescope about a single axis. Figure 2 depicts a typical concept of operational employment for the Bifocal Relay Mirror Spacecraft. The receive telescope acquires and tracks the source laser, while the transmit telescope tracks the target. The motion of the fast steering mirrors accomplished internal alignment and fine pointing of the beam on the target.

A. COORDINATE SYSTEM DEFINITION

The coordinate frame descriptions are with respect to Figure 3. The center of mass of the receive telescope is on the rotation axis. Therefore, the center of mass of the system is fixed during the relative motion of the receive telescope.

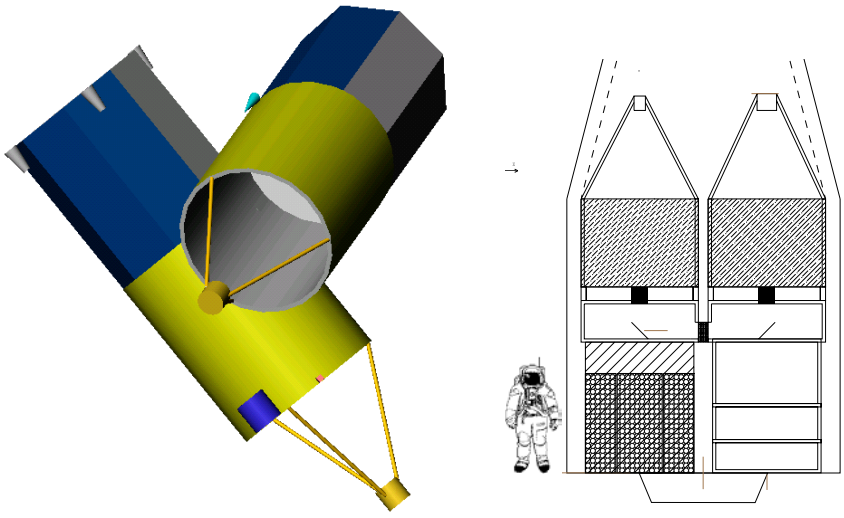

Figure 1 Bifocal Relay Mirror Spacecraft sketch (left) and relative size (right)

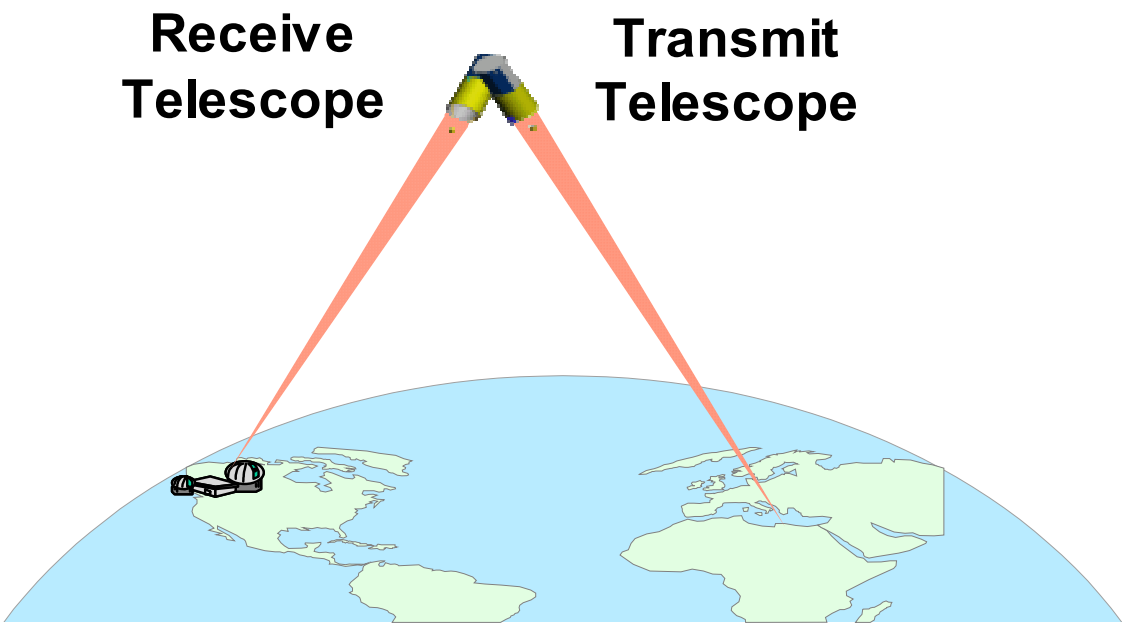

Figure 2 Concept of Operational Employment for Bifocal Relay Mirror Spacecraft

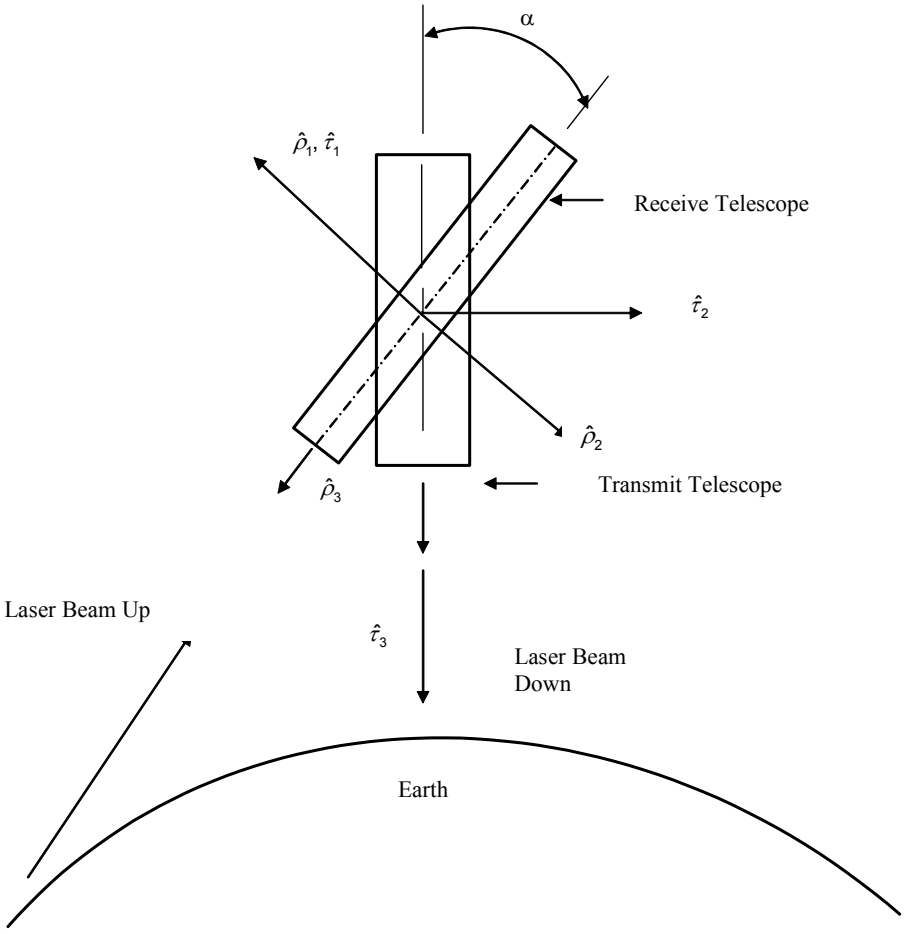

Figure 3 Bifocal Relay Mirror Spacecraft

The rigid body equations of motion for the transmitter and receiver are with respect to the inertial frame. Additionally, the dynamic coupling effects from the fast steering mirrors are neglected due to the small mass relative to the entire structure.

The coordinate system $\hat{\tau}_1, \hat{\tau}_2, \hat{\tau}_3$ is fixed in the transmit telescope with $\hat{\tau}_1$ axis parallel to rotation axis of the receive telescope, $\hat{\tau}_3$ as telescope axis and $\hat{\tau}_2$ is normal to $\hat{\tau}_1$ and $\hat{\tau}_3$ such that the $\hat{\tau}_1, \hat{\tau}_2, \hat{\tau}_3$ coordinate system is right-handed and mutually orthogonal frame. The origin of the coordinate system is at center of mass of the transmit telescope.

The coordinate system $\hat{\rho}_1, \hat{\rho}_2, \hat{\rho}_3$ is fixed in the receive system with $\hat{\rho}_1$ axis as the rotation axis, parallel to $\hat{\tau}_1$ axis, $\hat{\rho}_3$ as telescope and $\hat{\rho}_2$ is normal of $\hat{\rho}_1$ and $\hat{\rho}_3$ such that $\hat{\rho}_1, \hat{\rho}_2, \hat{\rho}_3'$ coordinate system is right-handed mutually orthogonal frame with origin at the center of mass of the receive telescope. The coordinate system $\hat{\rho}_1, \hat{\rho}_2, \hat{\rho}_3$ is obtained from the coordinate system $\hat{\tau}_1, \hat{\tau}_2, \hat{\tau}_3$ by rotation α about x-axis.

The relative motion of the transmit fast steering mirror with respect to transmit telescope is represented by β_x^τ rotation about $\hat{\tau}_1$ axis and β_y^τ rotation $\hat{\tau}_2$ axis. The relative motion of the receive fast steering mirror with respect to receive telescope is represented by β_x^ρ rotation about $\hat{\rho}_1$ axis and β_y^ρ rotation about $\hat{\rho}_2$ axis. The fast steering mirror rotations are assumed to be small. The equations of motion of the system are written in the coordinate frame $\hat{\tau}_1, \hat{\tau}_2, \hat{\tau}_3$.

B. EQUATIONS OF MOTION

In a general case, rotational equations of motion for a given body about an arbitrary point P are given by

Equation 1: Moment and Momentum Balance for Rigid Body

$$\vec{M}_p = \dot{\vec{H}}_p - \dot{\vec{\rho}}_c \times m \dot{\vec{r}}_c$$

where

$\vec{M}_p =$ total sum of external forces about P

$\dot{\vec{H}}_p =$ angular momentum of the body about P

$\rho_c =$ total vector from P to center of mass of the system

$m =$ total mass of the body

$\dot{r}_c =$ velocity of center of mass of the body

If the point P is the center of mass, then $\rho_c = 0$, then $\vec{M} = \dot{\vec{H}}|_N$, with N being used to indicate the inertial reference frame. The angular momentum of the system, H_S can be written as follows:

Equation 2: System Momentum Balance

$$\vec{H}_S = \vec{H} + \vec{H}_{rel} + \vec{H}_W$$

where

$\vec{H}_S =$ total angular momentum of the system.

$\vec{H} =$ total angular momentum by neglecting the contribution by the relative motion of the receive telescope and reaction wheels with respect to transmit telescope

$\vec{H}_{rel} =$ angular momentum due to relative motion of the receive telescope

$\vec{H}_W =$ angular momentum due to relative motion of the reaction wheels.

To continue the momentum derivation, we must determine the inertia properties of the system.

1. Inertia

Let I_τ be the inertia matrix of the transmit telescope about its center of mass in coordinate frame $\hat{\tau}_1, \hat{\tau}_2, \hat{\tau}_3$.

$$I_\tau = \begin{bmatrix} I_{xx}^\tau & -I_{xy}^\tau & -I_{xz}^\tau \\ -I_{yx}^\tau & I_{yy}^\tau & -I_{yz}^\tau \\ -I_{zx}^\tau & -I_{zy}^\tau & I_{zz}^\tau \end{bmatrix}$$

Let the vector from center of mass of the transmit telescope to the center of mass of the spacecraft is given by

$$\vec{r}^{B^*\tau} = x_\tau \hat{\tau}_1 + y_\tau \hat{\tau}_2 + z_\tau \hat{\tau}_3$$

Let I'_ρ be the inertia matrix of the receive telescope about its center of mass in coordinate frame $\hat{\rho}_1, \hat{\rho}_2, \hat{\rho}_3$. It is given by

$$I'_\rho = \begin{bmatrix} I_{x'x'}^\rho & -I_{x'y'}^\rho & -I_{x'z'}^\rho \\ -I_{y'x'}^\rho & I_{y'y'}^\rho & -I_{y'z'}^\rho \\ -I_{z'x'}^\rho & -I_{z'y'}^\rho & I_{z'z'}^\rho \end{bmatrix}$$

Next we transform I'_ρ to $\hat{\tau}_1, \hat{\tau}_2, \hat{\tau}_3$ frame. The transformation matrix from $\hat{\tau}_1, \hat{\tau}_2, \hat{\tau}_3$ to $\hat{\rho}_1, \hat{\rho}_2, \hat{\rho}_3$ is given by

$${}^\rho C^\tau = \begin{bmatrix} 1 & 0 & 0 \\ 0 & \cos(\alpha) & \sin(\alpha) \\ 0 & -\sin(\alpha) & \cos(\alpha) \end{bmatrix}$$

The transformation matrix ${}^\tau C^\rho$ from $\hat{\rho}_1, \hat{\rho}_2, \hat{\rho}_3$ to $\hat{\tau}_1, \hat{\tau}_2, \hat{\tau}_3$ is transpose of ${}^\rho C^\tau$. I'_ρ in $\hat{\tau}_1, \hat{\tau}_2, \hat{\tau}_3$ system, I_ρ, is given by $I_\rho = {}^\tau C^\rho I'_\rho {}^\rho C^\tau$

Let the vector from center of mass of the receive telescope to the center of mass of the system is given by

$$\vec{r}^{B^*\rho} = x_\rho \hat{\rho}_1 + y_\rho \hat{\rho}_2 + z_\rho \hat{\rho}_3$$

The inertia matrix of the spacecraft about its center of mass in coordinate frame $\hat{\tau}_1, \hat{\tau}_2, \hat{\tau}_3$ is given by

$$I_S = I_\tau + I_\rho + m_\tau \begin{bmatrix} y_\tau^2 + z_\tau^2 & -x_\tau y_\tau & -x_\tau z_\tau \\ -x_\tau y_\tau & z_\tau^2 + x_\tau^2 & -y_\tau z_\tau \\ -x_\tau z_\tau & -y_\tau z_\tau & x_\tau^2 + y_\tau^2 \end{bmatrix} + m_\rho \begin{bmatrix} y_\rho^2 + z_\rho^2 & -x_\rho y_\rho & -x_\rho z_\rho \\ -x_\rho y_\rho & z_\rho^2 + x_\rho^2 & -y_\rho z_\rho \\ -x_\rho z_\rho & -y_\rho z_\rho & x_\rho^2 + y_\rho^2 \end{bmatrix}$$

2. Angular Velocities

The inertial angular velocity of the transmit telescope is ${}^N\vec{\omega}^\tau = \begin{bmatrix} \omega_x & \omega_y & \omega_z \end{bmatrix}_\tau^T$. The relative angular velocity of the receive telescope with respect to transmit telescope is given by ${}^\tau\vec{\omega}^\rho = \begin{bmatrix} \dot{\alpha} & 0 & 0 \end{bmatrix}_\tau^T$. The inertial angular velocity of the receive telescope ${}^N\vec{\omega}^\rho = {}^N\vec{\omega}^\tau + {}^\tau\vec{\omega}^\rho = \begin{bmatrix} \omega_x + \dot{\alpha} & \omega_y & \omega_z \end{bmatrix}_\tau^T$.

3. Angular Momentum

The terms of Equation 2 are further defined below. The angular momentum without receive telescope relative motion is given by $\vec{H} = I_S\,{}^N\vec{\omega}^\tau$. The relative angular momentum is given by $\vec{H}_{rel} = I_\rho\,{}^\tau\vec{\omega}^\rho$.

Through substitution, we have

Equation 3: Refined System Momentum Balance

$$\vec{H}_S = I_S\,{}^N\vec{\omega}^\tau + I_\rho\,{}^\tau\vec{\omega}^\rho + \vec{H}_W$$

4. Kinematical Relationships

Using Equation 1, the equation of motion of the spacecraft is given by

Equation 4: Rigid Body Moment & Momentum Defined

$$\vec{M} = {}^N\frac{d}{dt}\vec{H}_S = {}^\tau\frac{d}{dt}\vec{H}_S + {}^N\vec{\omega}^\tau \times \vec{H}_S$$

where

${}^N\frac{d}{dt}\vec{H}_S$ = rate of change in inertial frame

$^{\tau}\frac{d}{dt}\vec{H}_S =$ rate of change in transmit telescope frame

It should be noted that since I_S is function of α, it is therefore time dependent.

a. Transmitter Kinematics

The momentum balance of the transmitter is as given as: $^{N}\vec{H}^{\tau} = I_{\tau}\,{}^{N}\vec{\omega}^{\tau} + \vec{h}_W$. The total moment applied to the transmitter is given by:

$$\vec{M}_{\tau} = \vec{M}_C + \vec{M}_G = {}^{N}\frac{d}{dt}{}^{N}\vec{H}^{\tau} = {}^{N}\frac{d}{dt}(I_{\tau}\,{}^{N}\vec{\omega}^{\tau} + \vec{h}_W)$$

$$\cdots = {}^{\tau}\frac{d}{dt}(I_{\tau}\,{}^{N}\vec{\omega}^{\tau} + \vec{h}_W) + {}^{N}\vec{\omega}^{\tau} \times (I_{\tau}\,{}^{N}\vec{\omega}^{\tau} + \vec{h}_W)$$

$$\cdots = (I_{\tau}\,{}^{N}\dot{\vec{\omega}}^{\tau} + \dot{\vec{h}}_W) + {}^{N}\vec{\omega}^{\tau} \times (I_{\tau}\,{}^{N}\vec{\omega}^{\tau} + \vec{h}_W)$$

The subscripts C and G represent Control and Gimbal, respectively. The gimbal torque is due to the relative motion of the two telescopes. The receiver momentum is given by $^{N}\vec{H}^{\rho} = I_{\rho}\,{}^{N}\vec{\omega}^{\rho} = {}^{\tau}C^{\rho} I_{\rho}\,{}^{\rho}C^{\tau}({}^{N}\vec{\omega}^{\tau} + {}^{\tau}\vec{\omega}^{\rho}) = {}^{\tau}C^{\rho} I_{\rho}\,{}^{\rho}C^{\tau}({}^{N}\vec{\omega}^{\tau} + \dot{\vec{\alpha}})$. The moment applied to the receiver is given by:

$$\vec{M}_{\rho} = -\vec{M}_G = {}^{N}\frac{d}{dt}{}^{N}\vec{H}^{\rho} = {}^{N}\frac{d}{dt}({}^{\tau}C^{\rho} I_{\rho}\,{}^{\rho}C^{\tau}({}^{N}\vec{\omega}^{\tau} + \dot{\vec{\alpha}}))$$

$$\cdots = {}^{\tau}\frac{d}{dt}({}^{\tau}C^{\rho} I_{\rho}\,{}^{\rho}C^{\tau}({}^{N}\vec{\omega}^{\tau} + \dot{\vec{\alpha}})) + {}^{N}\vec{\omega}^{\tau} \times {}^{\tau}C^{\rho} I_{\rho}\,{}^{\rho}C^{\tau}({}^{N}\vec{\omega}^{\tau} + \dot{\vec{\alpha}})$$

$$\cdots = ({}^{\tau}\dot{C}^{\rho} I_{\rho}\,{}^{\rho}C^{\tau} + {}^{\tau}C^{\rho} I_{\rho}\,{}^{\rho}\dot{C}^{\tau})({}^{N}\vec{\omega}^{\tau} + \dot{\vec{\alpha}}) + {}^{\tau}C^{\rho} I_{\rho}\,{}^{\rho}C^{\tau}({}^{N}\dot{\vec{\omega}}^{\tau} + \ddot{\vec{\alpha}})$$

$$\cdots + {}^{N}\vec{\omega}^{\tau} \times {}^{\tau}C^{\rho} I_{\rho}\,{}^{\rho}C^{\tau}({}^{N}\vec{\omega}^{\tau} + \dot{\vec{\alpha}})$$

System-level open-loop control input is achieved through system-level dynamic equilibrium, as follows.

Equation 5: Open-Loop Control Torque

$$\vec{M}_C = -\vec{M}_G + (\vec{M}_C + \vec{M}_G) = \vec{M}_\rho + \vec{M}_\tau$$
$$\cdots = \{({}^\tau\dot{C}^\rho I_\rho {}^\rho C^\tau + {}^\tau C^\rho I_\rho {}^\rho\dot{C}^\tau)({}^N\vec{\omega}^\tau + \dot{\vec{\alpha}}) + {}^\tau C^\rho I_\rho {}^\rho C^\tau({}^N\dot{\vec{\omega}}^\tau + \ddot{\vec{\alpha}})$$
$$\cdots + {}^N\vec{\omega}^\tau \times {}^\tau C^\rho I_\rho {}^\rho C^\tau({}^N\vec{\omega}^\tau + \dot{\vec{\alpha}})\} + \{I_\tau {}^N\dot{\vec{\omega}}^\tau + {}^N\vec{\omega}^\tau \times (I_\tau {}^N\vec{\omega}^\tau + \vec{h}_W)\}$$
$$\cdots = \dot{I}_\rho({}^N\vec{\omega}^\tau + \dot{\vec{\alpha}}) + I_S {}^N\dot{\vec{\omega}}^\tau + {}^N\vec{\omega}^\tau \times (I_S {}^N\vec{\omega}^\tau + \vec{h}_W + {}^\tau C^\rho I_\rho {}^\rho C^\tau\dot{\vec{\alpha}}) + {}^\tau C^\rho I_\rho {}^\rho C^\tau\ddot{\vec{\alpha}}$$

In later chapters, it will become necessary to have the acceleration of the telescopes in order to determine the effects of flexibility. Given that attitude and angular rates are observable with most sensors, the above equation may be solved for ${}^N\dot{\vec{\omega}}^\tau$.

Equation 6: Angular Acceleration of Transmitter

$${}^N\dot{\vec{\omega}}^\tau = I_{TOTAL}{}^{-1}(\vec{M}_C - {}^N\vec{\omega}^\tau \times (I_{TOTAL} {}^N\vec{\omega}^\tau + \vec{h}_W + {}^\tau C^\rho I_\rho {}^\rho C^\tau\dot{\vec{\alpha}}) - \dot{I}_\rho({}^N\vec{\omega}^\tau + \dot{\vec{\alpha}}) - {}^\tau C^\rho I_\rho {}^\rho C^\tau\ddot{\vec{\alpha}})$$

b. Receiver Kinematics

The inertial angular acceleration of the receiver is simply ${}^N\dot{\vec{\omega}}^\rho = {}^N\dot{\vec{\omega}}^\tau + \ddot{\vec{\alpha}}$.

Equation 7: Angular Acceleration of Receiver

$${}^N\dot{\vec{\omega}}^\rho = {}^N\dot{\vec{\omega}}^\tau + \ddot{\vec{\alpha}}$$
$$\cdots = I_{TOTAL}{}^{-1}(\vec{M}_C - {}^N\vec{\omega}^\tau \times (I_{TOTAL} {}^N\vec{\omega}^\tau + \vec{h}_W + {}^\tau C^\rho I_\rho {}^\rho C^\tau\dot{\vec{\alpha}}) - \dot{I}_\rho({}^N\vec{\omega}^\tau + \dot{\vec{\alpha}}) - {}^\tau C^\rho I_\rho {}^\rho C^\tau\ddot{\vec{\alpha}}) + \ddot{\vec{\alpha}}$$

5. Wheel Control Laws

Reaction wheels are typically controlled by a proportional-derivative (PD) controller of the form $\dot{H}_{Wi} = 2\ k_i q_{iE} q_{4E} + k_{id}\omega_{iE}$. This control law is developed in Wie. Where q_{iE} is the ith element of the error quaternion and ω_{iE} is the error between commanded and measured angular rate about the ith axis. The PD controller used in this work is of the same form, but with the parameters defined differently. The feedback control law used in this work is shown in Equation 8.

Equation 8: Proportional Derivative Controller

$$\dot{H}_{Wi} = k_i(q_{iE} q_{4E} + \tau_i\omega_{iE})$$

Where k_i is the controller gain and τ_i is the controller time constant. This creates a dynamic situation of the form $I_i\dot{\omega} + k_i\tau_i\omega_{iE} + k_i q_{iE} q_{4E} = 0$. The bandwidth of the controller goes as the square root of k_i. Hence, increasing the bandwidth by a factor of two requires increasing the gain by a factor of four.

6. Commanded Trajectory

The commanded trajectory for this control system is based upon initial conditions for the joint angle motion as well as the transmitter acceleration and rates. The initial quaternion for the transmit telescope is given by $q_\tau(t_0)$. The initial transmit telescope inertial angular velocity is given by ${}^N\vec{\omega}^\tau(t_0)$. The initial joint angle is given by $\alpha(t_0)$. The initial joint angle is given by $\dot{\alpha}(t_0)$.

Equation 9: Initial Conditions for Simulations

$$q_\tau(t_0) = \begin{bmatrix} 0 \\ 0 \\ 0 \\ 1 \end{bmatrix}$$

$${}^N\vec{\omega}^\tau(t_0) = \begin{bmatrix} 0 \\ 0 \\ 0 \end{bmatrix} rad/\sec$$

$$\alpha(t_0) = 0\ rad$$

$$\dot{\alpha}(t_0) = 0\ rad/\sec$$

The commanded attitude profile is based upon a typical engagement scenario. The inertial acceleration for the transmit telescope and the relative acceleration for the receive telescope is taken from the existing simulation. The values are described in Equation 10.

Equation 10: Commanded Acceleration Profile for Simulations

$${}^N\dot{\vec{\omega}}^\tau(t) = \begin{bmatrix} 0.308\sin(0.0079t) \\ 7.896\sin(0.0126t) \\ -1.097\sin(0.0105t) \end{bmatrix} x10^{-5}\ rad/\sec^2$$

$$\ddot{\alpha}(t) = 1.1484\sin(0.0209t)x10^{-4}\ rad/\sec^2$$

THIS PAGE INTENTIONALLY LEFT BLANK

III. MULTI-BODY FLEXIBLE EQUATIONS OF MOTION

A. FLEXIBLE EQUATIONS OF MOTION – GENERAL CASE

Given: flexible body, with a cantilevered attachment at point A, the equations of motion may be stated as follows:

Equation 11: Cantilevered Dynamics

$$\begin{bmatrix} M_{II} & M_{IA} \\ M_{AI} & M_{AA} \end{bmatrix} \begin{Bmatrix} \ddot{U}_I \\ \ddot{U}_A \end{Bmatrix} + \begin{bmatrix} K_{II} & K_{IA} \\ K_{AI} & K_{AA} \end{bmatrix} \begin{Bmatrix} U_I \\ U_A \end{Bmatrix} = \begin{Bmatrix} F_I \\ F_A \end{Bmatrix}$$

Where

I ≡ Internal Nodes

A ≡ Attachment Point

M & K ≡ Mass & Stiffness Matrices from cantilevered condition in finite element analysis program

Equation 12: Transfer Nodes to Modal Coordinates

$$\textbf{Let} \begin{Bmatrix} U_I \\ U_A \end{Bmatrix} = \begin{bmatrix} \Phi_E & \Phi_R \\ 0 & I \end{bmatrix} \begin{Bmatrix} q_A \\ U_A \end{Bmatrix}$$

Where q_A are modal coordinates at the attachment and Φ_E is normalized for unity modal masses, i.e. $\Phi_E{}^T M_{II} \Phi_E = I$. The terms modal coordinates and generalized coordinates are interchangeable for the purposes used in this document.

Substitute Equation 12 into Equation 11 and premultiply by $\begin{bmatrix} \Phi_E{}^T & 0 \\ \Phi_R{}^T & I \end{bmatrix}$ to get:

Equation 13: Dynamics Expressed in Modal and Attachment Coordinates

$$\begin{bmatrix} I & M_{AE} \\ M_{AE}{}^T & M_{AR} \end{bmatrix} \begin{Bmatrix} \ddot{q}_A \\ \ddot{U}_A \end{Bmatrix} + \begin{bmatrix} \omega^2 & 0 \\ 0 & 0 \end{bmatrix} \begin{Bmatrix} q_A \\ U_A \end{Bmatrix} = \begin{Bmatrix} \bar{F}_I \\ \bar{F}_A \end{Bmatrix}$$

Where,

$$M_{AE} = \Phi_E{}^T M_{II} \Phi_R + \Phi_E{}^T M_{IA}$$
$$M_{AR} = \Phi_R{}^T M_{II} \Phi_R + M_{AI} \Phi_R + \Phi_R{}^T M_{IA} + M_{AA}$$
$$\omega^2 = \Phi_E{}^T K_{II} \Phi_E$$
$$\bar{F}_I = \Phi_E{}^T F_I$$
$$\bar{F}_A = \Phi_R{}^T F_I + F_A$$

Equation 13 is general in nature, and specific to the coordinates of the flexible body. The next series of equation transforms Equation 13 from coordinates at the cantilevered appendage to a common coordinate system with a given location and orientation. The selected coordinate system is defined as the axes defined by the transmit telescope coordinate system, located at the system center of mass, B^*. This basis is called {B}, as it is the body coordinate system use. The transmitter basis and the body basis differ in origin, but not orientation. The radius vectors from the B^* to the attachment points of the transmitter and receiver are given by:

Equation 14: Center of Mass Locations

$$\vec{r}^{B^*\tau} = x_\tau \hat{\tau}_1 + y_\tau \hat{\tau}_2 + z_\tau \hat{\tau}_3$$
$$\vec{r}^{B^*\rho} = x_\rho \hat{\rho}_1 + y_\rho \hat{\rho}_2 + z_\rho \hat{\rho}_3$$

The attachment coordinates are expanded to divide between transmitter and receiver coordinates, superscripted by τ and ρ respectively. Translation and rotation are indicated by lower case t and r respectively. For each flexible body $\{U_A\} = \{U_A^t \quad U_A^r\}^T$. Hence, the translational and rotational attachment coordinates may be expressed in terms of the body coordinates as follows.

Equation 15: Coordinate Transformations

$$\begin{Bmatrix} U_A^t \\ U_A^r \end{Bmatrix} = \begin{bmatrix} C_A & 0 \\ 0 & C_A \end{bmatrix} \begin{bmatrix} I & R \\ 0 & I \end{bmatrix} \begin{Bmatrix} U^t \\ U^r \end{Bmatrix} = \begin{bmatrix} C_A & C_A R \\ 0 & C_A \end{bmatrix} \begin{Bmatrix} U^t \\ U^r \end{Bmatrix} = [T]\{U\}$$

where

$$[R] = \begin{bmatrix} 0 & z_A & -y_A \\ -z_A & 0 & x_A \\ y_A & -x_A & 0 \end{bmatrix}$$

Substitute Equation 15 into Equation 13 and premultiply by $\begin{bmatrix} I & 0 \\ 0 & T^T \end{bmatrix}$ to obtain

Equation 16: EOMs in Modal and Body Coordinates

$$\begin{bmatrix} I & M_{AEO} \\ M_{AEO}{}^T & M_{ARO} \end{bmatrix} \begin{Bmatrix} \ddot{q}_A \\ \ddot{U} \end{Bmatrix} + \begin{bmatrix} \omega^2 & 0 \\ 0 & 0 \end{bmatrix} \begin{Bmatrix} q_A \\ U \end{Bmatrix} = \begin{Bmatrix} \bar{F}_{AI} \\ \bar{F}_{AO} \end{Bmatrix}$$

where

$M_{AEO} = M_{AE} T$

$M_{ARO} = T^T M_{AR} T$

$\bar{F}_{AI} = \bar{F}_I$

$\bar{F}_{AO} = T^T \bar{F}_A$

$U = \begin{Bmatrix} U^T \\ U^R \end{Bmatrix}$

B. FLEXIBLE EQUATIONS OF MOTION – TRANSMIT TELESCOPE

Flexible Body Equations of Motion for Transmit Telescope (Note: A replaced by τ)

Coordinate Transfer:

$\{T\} = {}^{\tau}C^B \{B\}$

$\begin{Bmatrix} \tau_1 \\ \tau_2 \\ \tau_3 \end{Bmatrix} = \begin{Bmatrix} b_1 \\ b_2 \\ b_3 \end{Bmatrix}$

${}^{\tau}C^B = I$

Equation 17: Transformation and Mass Matrices, Transmit Telescope

$$[T_\tau] = \begin{bmatrix} 1 & 0 & 0 & 0 & z_\tau & -y_\tau \\ 0 & 1 & 0 & -z_\tau & 0 & x_\tau \\ 0 & 0 & 1 & y_\tau & -x_\tau & 0 \\ 0 & 0 & 0 & 1 & 0 & 0 \\ 0 & 0 & 0 & 0 & 1 & 0 \\ 0 & 0 & 0 & 0 & 0 & 1 \end{bmatrix} = \begin{bmatrix} I & R_\tau \\ 0 & I \end{bmatrix}$$

$$[M_{\tau R}] = \begin{bmatrix} m_\tau & 0 & 0 & 0 & 0 & 0 \\ 0 & m_\tau & 0 & 0 & 0 & 0 \\ 0 & 0 & m_\tau & 0 & 0 & 0 \\ 0 & 0 & 0 & I^\tau_{xx} & I^\tau_{xy} & I^\tau_{xz} \\ 0 & 0 & 0 & I^\tau_{xy} & I^\tau_{yy} & I^\tau_{yz} \\ 0 & 0 & 0 & I^\tau_{xz} & I^\tau_{yz} & I^\tau_{zz} \end{bmatrix} = \begin{bmatrix} M_\tau & 0 \\ 0 & I^\tau \end{bmatrix}$$

$$[M_{\tau RO}] = T_\tau^T M_{\tau R} T_\tau = \begin{bmatrix} M_\tau & M_\tau R_\tau \\ R_\tau^T M_\tau & R_\tau^T M_\tau R_\tau + I^\tau \end{bmatrix}$$

C. FLEXIBLE EQUATIONS OF MOTION – RECEIVE TELESCOPE

Flexible Body Equations of Motion for Receive Telescope (Note: A replaced by ρ)

Coordinate Transfer:

$$\{R\} = {}^\rho C^B \{B\}$$

$$\begin{Bmatrix} \rho_1 \\ \rho_2 \\ \rho_3 \end{Bmatrix} = \begin{bmatrix} 1 & 0 & 0 \\ 0 & \cos(\alpha) & \sin(\alpha) \\ 0 & -\sin(\alpha) & \cos(\alpha) \end{bmatrix} \begin{Bmatrix} b_1 \\ b_2 \\ b_3 \end{Bmatrix}$$

$${}^\rho C^B = \begin{bmatrix} 1 & 0 & 0 \\ 0 & \cos(\alpha) & \sin(\alpha) \\ 0 & -\sin(\alpha) & \cos(\alpha) \end{bmatrix}$$

Equation 18: Transformation and Mass Matrices, Receive Telescope

$$\left[T_\rho\right] = \begin{bmatrix} {}^{\rho}C^{B} & {}^{\rho}C^{B}R_\rho \\ 0 & {}^{\rho}C^{B} \end{bmatrix}$$

$$= \begin{bmatrix} 1 & 0 & 0 & 0 & z_\rho & -y_\rho \\ 0 & \cos(\alpha) & \sin(\alpha) & y_\rho\sin(\alpha) - z_\rho\cos(\alpha) & -x_\rho\sin(\alpha) & x_\rho\cos(\alpha) \\ 0 & -\sin(\alpha) & \cos(\alpha) & y_\rho\cos(\alpha) + z_\rho\sin(\alpha) & -x_\rho\cos(\alpha) & -x_\rho\sin(\alpha) \\ 0 & 0 & 0 & 1 & 0 & 0 \\ 0 & 0 & 0 & 0 & \cos(\alpha) & \sin(\alpha) \\ 0 & 0 & 0 & 0 & -\sin(\alpha) & \cos(\alpha) \end{bmatrix}$$

$$\left[M_{\rho R}\right] = \begin{bmatrix} m_\rho & 0 & 0 & 0 & 0 & 0 \\ 0 & m_\rho & 0 & 0 & 0 & 0 \\ 0 & 0 & m_\rho & 0 & 0 & 0 \\ 0 & 0 & 0 & I^{\rho}_{xx} & I^{\rho}_{xy} & I^{\rho}_{xz} \\ 0 & 0 & 0 & I^{\rho}_{xy} & I^{\rho}_{yy} & I^{\rho}_{yz} \\ 0 & 0 & 0 & I^{\rho}_{xz} & I^{\rho}_{yz} & I^{\rho}_{zz} \end{bmatrix} = \begin{bmatrix} M_\rho & 0 \\ 0 & I^{\rho} \end{bmatrix}$$

$$\left[M_{\rho RO}\right] = T_\rho^{T} M_{\rho R} T_\rho = \begin{bmatrix} {}^{\rho}C^{BT} M_\rho {}^{\rho}C^{B} & {}^{\rho}C^{BT} M_\rho {}^{\rho}C^{B} R_\rho \\ R_\rho^{T} {}^{\rho}C^{BT} M_\rho {}^{\rho}C^{B} & R_\rho^{T} {}^{\rho}C^{BT} M_\rho {}^{\rho}C^{B} R_\rho + {}^{\rho}C^{BT} I^{\rho} {}^{\rho}C^{B} \end{bmatrix}$$

Now, we have M_{ARO} for transmit and receive, we need M_{AEO} for transmit and receive. See Equation 16. These rigid-elastic coupling matrices are available from most of the widely used finite element analysis programs, such as NASTRAN or I-DEAS.

THIS PAGE INTENTIONALLY LEFT BLANK

IV. STRUCTURE-CONTROLS INTERACTION

In order to control the motion of flexible structures consisting of rigid body and elastic motion, the coupling between rigid body motion and elastic motion is important. Controlling the rigid body attitude is one of the primary objectives. Initially, the objective of achieving fine pointing may drive the control design to a simple, high gain controller. That is, retain the commonly used PD control architecture with higher proportional gain. This provides more control authority based to control attitude errors. If the designer increases the proportional gain by a factor of four, the control bandwidth doubles. This was discussed when Equation 8 was presented. If this high gain controller is within the structural frequency, the structural modes will get excited. Given the rigid-body model, the gain would be set in order to achieve the design-specific pointing accuracy. Ultimately, that is how the PD gains would be adjusted to achieve high pointing accuracy. The question is: how do we modify the controller to behave favorably around the structural frequencies?

A. COMPENSATOR DESIGN

Compensators are applied after the rigid body control is applied. The purpose of the compensator is to add stability to the system. The stability is with respect to gain, phase, or a combination. Classical gain-phase stabilization techniques are of primary use to single-input single-output (SISO) systems. A rigid or flexible body is said to be gain-phase stabilized if it is closed loop stable with finite gain and phase margins. These classical techniques will be applied to this multi-input multi-output (MIMO) system [Ref Wie].

1. Gain Stabilization

Gain stabilization of a flexible body attenuates the gain at desired frequencies, to provide closed loop stability regardless of phase uncertainty. A gain stabilized mode has a finite gain margin, but is closed loop stable regardless of the phase uncertainty.

2. Phase Stabilization

Phase stabilization of a flexible body provides phase characteristics at the desired frequency to obtain closed loop damping higher than the passive damping of the mode. A phase stabilized mode has a finite phase margin, but is closed loop stable regardless of the loop gain uncertainty. Since the dynamic model has no passive damping, phase stabilization is required for this application.

B. COMMON CLASSICAL COMPENSATOR DESIGN

Wie presents a comprehensive discussion compensator design in his book. One fundamental concept is that gain stabilization may only be achieved if the corresponding mode has some passive damping. Since no modal damping is modeled, phase stabilization techniques must be employed. The following sections highlight some common compensator designs.

Control theory has made significant advances in the past several decades. Application of these theories has been difficult, from a practicality perspective. More often than not, classical techniques are applied. Performance is "optimized" through trial and error synthesis using frequency domain methods or actual performance in situ. Due to the complexity of the dynamic model, performance will be compared based on the performance of the plant under various compensation techniques. For lower performance requirements, simple first order filters are sufficient. The effect of the first order filter is to change the controller bandwidth. Typically, low pass filters are used for this type of an application, since they will eliminate the high frequency content of the controller, hence not exciting the structural modes. However, for higher performance requirements, such as placing the control bandwidth close to or within the structural modes, higher order filters become necessary.

Wie presents the generalized second order filter, using the s-domain. He presents it as a natural extension of the classical notch or phase lead/lag filter, and is based on pole-zero patterns. The following sections employ Wie's descriptions for various compensation methods. The filter is of the form:

Equation 19: Generalized Second-Order Filter, Ref Wie

$$H(s) = \frac{\frac{s^2}{\omega_z^2} + \frac{2\zeta_z s}{\omega_z} + 1}{\frac{s^2}{\omega_p^2} + \frac{2\zeta_p s}{\omega_p} + 1}$$

1. Minimum-Phase Lead Filter

A phase-lead filter utilizes Equation 19, and assigns $\zeta_c \equiv \zeta_z = \zeta_p > 0$. The maximum phase lead, obtained at $\omega_c = \sqrt{\omega_z \omega_p}$, is determined by:

Equation 20: Maximum Phase from a Phase Lead Filter, Ref Wie

$$\phi_{\max} = \cos^{-1}\left[\frac{\left(2\zeta_c\sqrt{\omega_p/\omega_z}\right)^2 - \left(\omega_p/\omega_z - 1\right)^2}{\left(2\zeta_c\sqrt{\omega_p/\omega_z}\right)^2 + \left(\omega_p/\omega_z - 1\right)^2}\right], \text{ at } \omega_c = \sqrt{\omega_z\omega_p}$$

The gain increases or decreases at high frequencies, and becomes $K_\infty = 40\log_{10}(\omega_p/\omega_z)$ *dB*. For small ζ_c, when filter poles and zeros are close to the imaginary axis, the effective lag region lies between ω_z *and* ω_p, and the maximum phase shift approaches ±180°. In practice, ζ_p is often selected greater than ζ_z. This places the filter poles sufficiently far to the left of the imaginary axis. The use of a phase-lag filter with a large ω_z/ω_p ratio greater than two should be avoided from a practical viewpoint. The phase lag filter is shown in Figure 4.

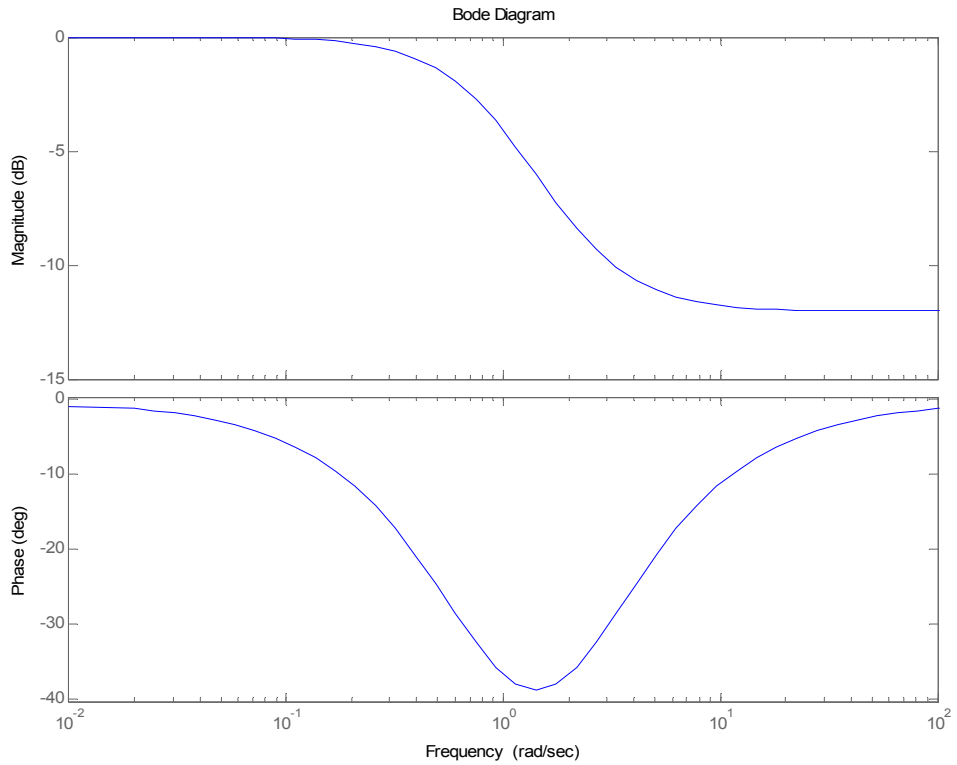

Figure 4 Bode Plot of Minimum-Phase Lag Filter

2. Minimum-Phase Notch Filter

For $\omega_p = \omega_z$, a notch filter is obtained. The minimum gain of the filter is obtained at $\omega_c \equiv \omega_z = \omega_p$ as $K_\infty = 20\log_{10}(\zeta_z / \zeta_p)$ dB. Both phase lead and lag occur near ω_c. For the notch filter, the maximum phase lag and lead occur at ω_1 and ω_2, respectively, where:

Equation 21: Location of Maximum Phase Lead or Lag for Notch Filter, Ref Wie

$$\frac{\omega_1}{\omega_c} = \sqrt{2\zeta_z\zeta_p + 1 - \sqrt{\left(2\zeta_z\zeta_p + 1\right)^2 - 1}}$$

$$\frac{\omega_2}{\omega_c} = \sqrt{2\zeta_z\zeta_p + 1 + \sqrt{\left(2\zeta_z\zeta_p + 1\right)^2 - 1}}$$

Because $\frac{\omega_1}{\omega_c}$ *and* $\frac{\omega_2}{\omega_c}$ depend only on the product $\zeta_z\zeta_p$, the filter damping ratios determine the effective notch region. Typical notch filter damping ratios are $\zeta_z = 0, \textit{and}\ \zeta_p = 1$. The minimum phase notch filter is shown in Figure 5.

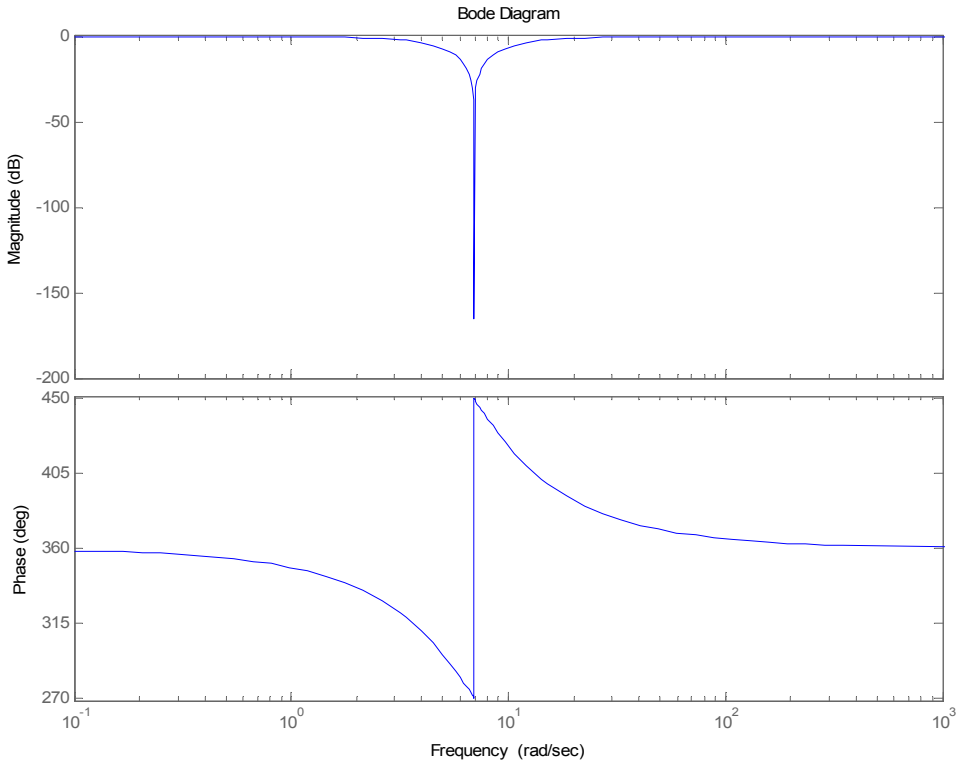

Figure 5 Bode Plot of Minimum Phase Notch Filter

3. Nonminimum-Phase Notch Filter

For $\omega_z = \omega_p$, and $\zeta_p > |\zeta_z| \ (\zeta_z < 0)$, a nonminimum-phase notch filter is realized. The applicability of this filter is when passive damping does not exist (the ideal case). The conventional notch filter cannot be used in this case. As the pole-zero combination is placed further from the imaginary axis, the robustness of the filter is enhanced, while the stability margin is reduced. The nonminimum phase notch filter is shown in Figure 6.

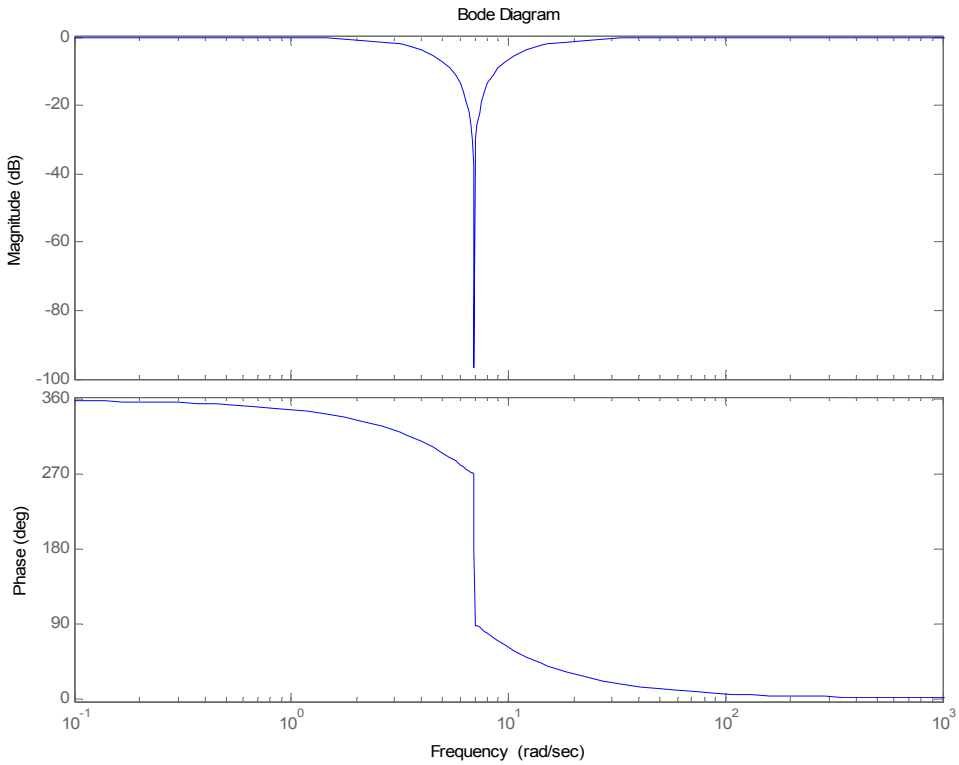

Figure 6 Bode Plot of Noninimum Phase Notch Filter

C. CLASSICAL COMPENSATOR DESIGN

Wie presents an algorithm for designing compensators with generalized filters. The basic idea is to synthesize the compensator for one mode at a time. The design algorithm is summarized below:

1. Select Control Bandwidth

The driving control bandwidth is one of the key parameters of the design. This may be driven by performance, noise sensitivity, control authority, etc.

2. Rigid Body Mode Compensation

Rigid body control is typically achieved through a proportional-derivative (PD) feedback controller. The format of the control law is given by: $u = -K(1+Ts)y = -(K_P + K_D s)y$.

3. Flexible Mode Compensation

The types and degrees of the closed loop behavior depend on the relative spectral separation of the modes. Determine if simple gain stabilization of all the flexible modes are possible. If not, determine the needed lead or lag angles foe each mode. Synthesize the appropriate structural filter for each destabilizing mode one by one, using the various second-order filters.

4. Design Iteration

Repeat the process to compromise the interactions between each compensator. A few iterations using a software package, or analytical model, will result in a more streamlined design process.

THIS PAGE INTENTIONALLY LEFT BLANK

V. DEVELOPMENT AND VALIDATION ANALYTICAL MODEL

A. FLEXIBILITY SIMULATION ARCHITECTURE

Now that the flexible telescopes are modeled dynamically, a method of simulation must be developed. The approach used is the feedback torque effect. This method is presented in simple terms in Figure 7. In essence, the rigid body dynamics are unchanged. However, the state vector determines the base excitation (acceleration) which creates a feedback torque. This feedback torque is combined with the control torque to affect the rigid body dynamics.

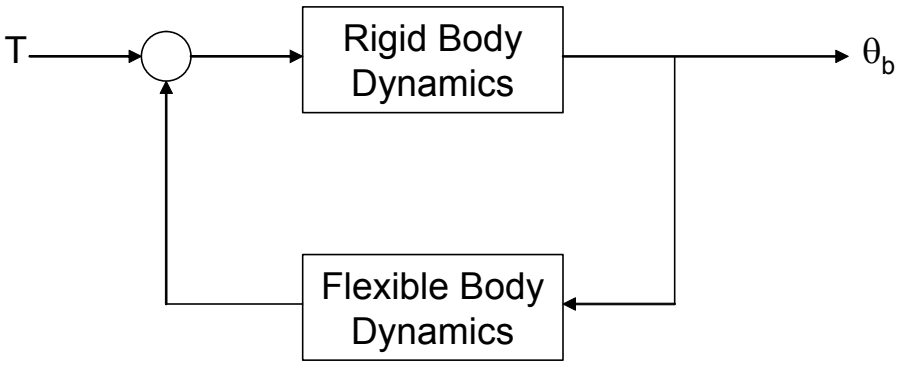

Figure 7 Flexibility Model, After Ref Agrawal

In Figure 7, T represents the command input (Torque), and θ_b represents the state vector. Using Equation 16 as a reference, the general equation that we are solving is of the form $A\ddot{x} + Bx = F$, where x = [q, U]^T. The most practical and mathematically stable method of solving this system of equations is to determine the rigid body state and work backwards to determine the reaction torque which results from the flexibility. This is shown in the next series of equations. If we start with Equation 16 as a base equation, the known values are the mass and stiffness matrices, as well as $\ddot{U}$ and q_A. We may restate Equation 16 as two differential algebraic equations, as in Equation 22.

Equation 22: Application of Equation 16 for Determining Simulation Algorithm

$$I\ddot{q}_A + M_{AEO}\ddot{U} + \omega^2 q_A = 0$$

$$M_{AEO}{}^T\ddot{q}_A + M_{ARO}\ddot{U} = T_A$$

Through reorganization, Equation 22 may be restated as

Equation 23: Determining Reaction Torque

$$\ddot{q}_A = -M_{AEO}\ddot{U} - \omega^2 q_A$$

$$T_{reaction} = -(M_{AEO}{}^T\ddot{q}_A + M_{ARO}\ddot{U})$$

At first, it isn't intuitive why the second equation has the negative sign. Without that negative sign, the system is unstable. With the negative sign, the system behaves as it should. In plain verbiage, the negative sign is there because it is a reaction torque, the behavior of which opposes that of an applied torque. The generalized coordinates are initialized at zero when the simulation begins. The stable algorithm for determining the reaction torque is shown in depicted in Figure 8.

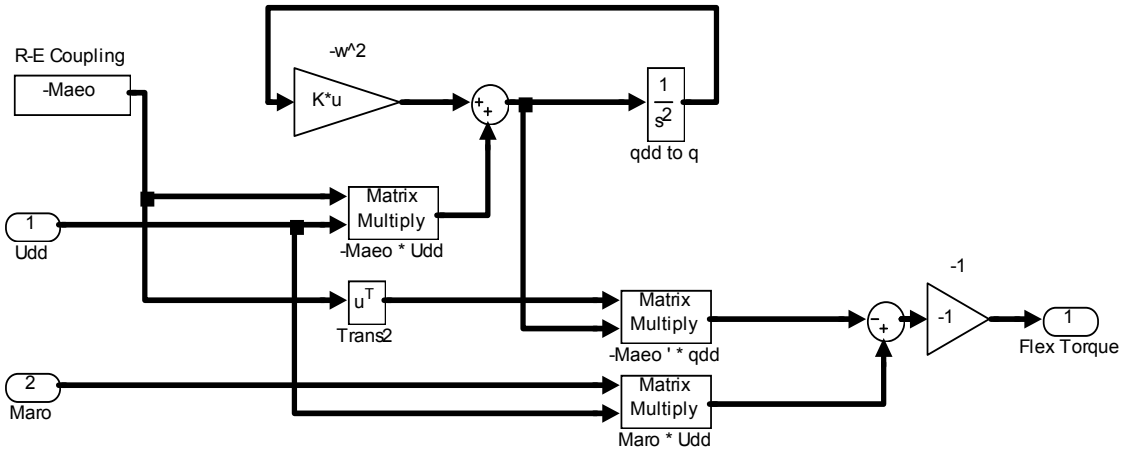

Figure 8 Determining Feedback Torque from Rigid Body Motion

B. DYNAMICAL SIMULATION DEVELOPMENT

The base acceleration is determined using Equation 6 and Equation 7 for the transmitter and receiver, respectively. The block diagram in Figure 9 shows how to determine the inertial acceleration of each body from the observed states,

using Equation 6 and Equation 7. The block diagram in Figure 10 determines the feedback torque due to flexibility, using Equation 23.

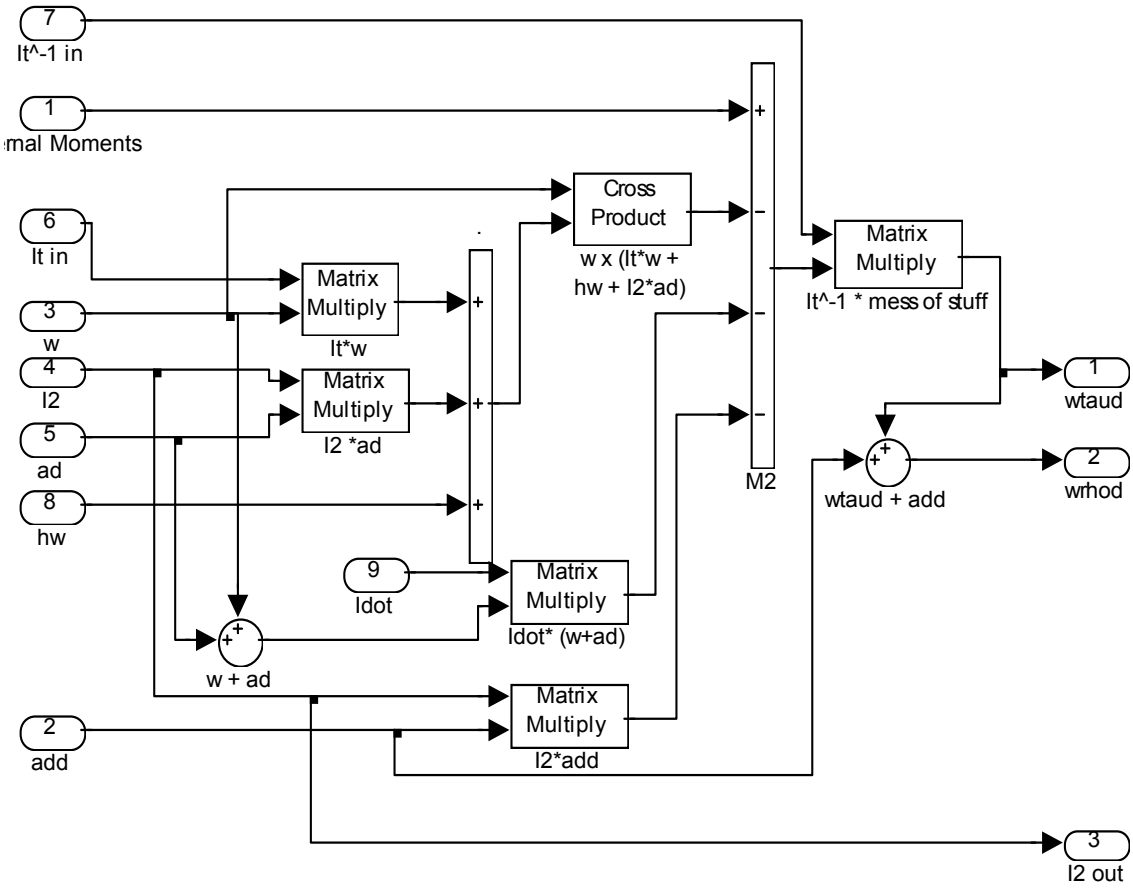

Figure 9 SIMULINK Model for Determining Rigid Body Acceleration of Transmitter and Receiver, using Equation 22 and Equation 23

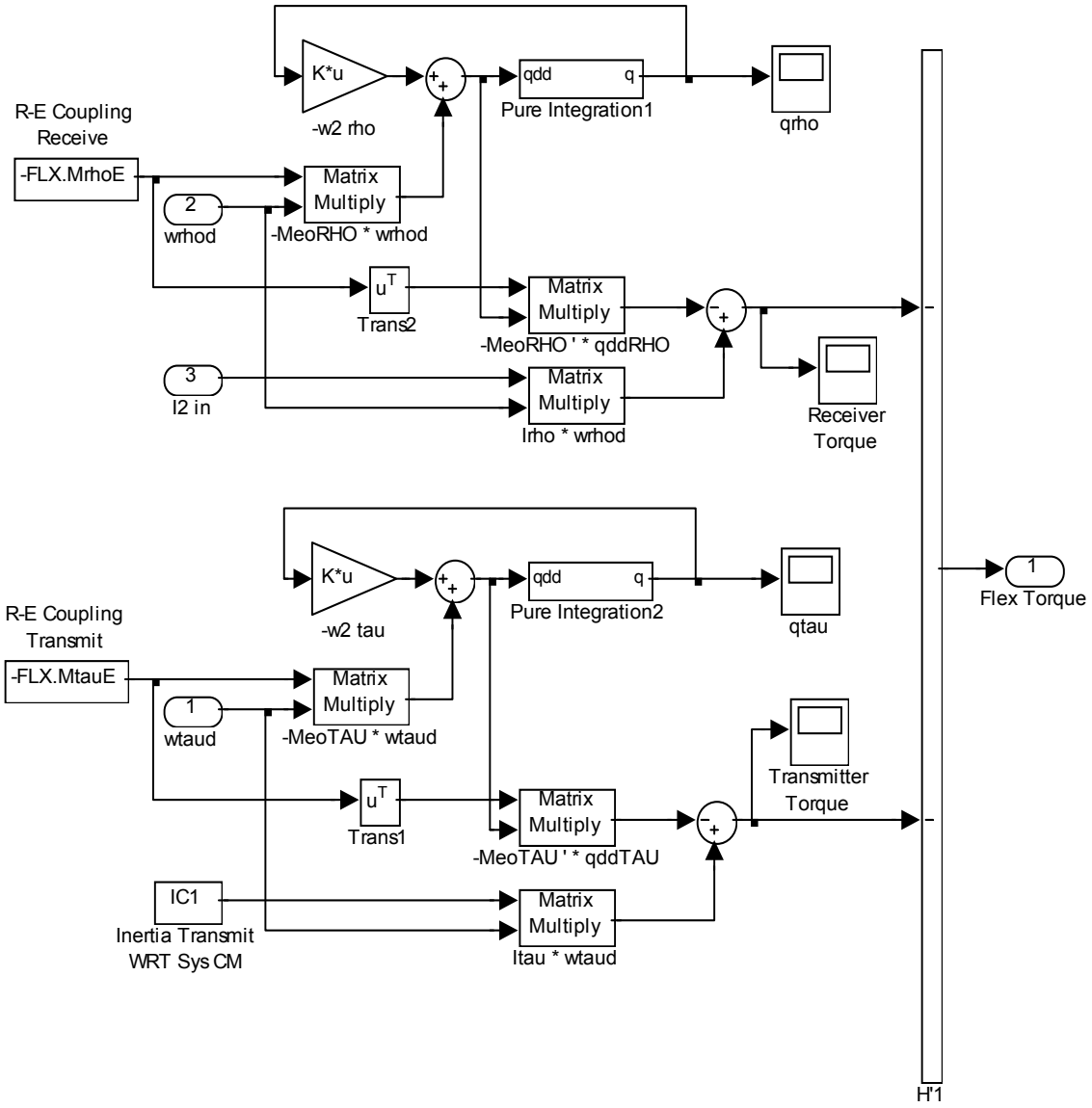

Figure 10 SIMULINK Model for Determining Torque Due to Acceleration of Flexible Bodies, using Equation 23

C. VALIDATION OF DYNAMICAL MODEL

1. Developing Flexible Bodies

The MSC software suites of PATRAN and NASTRAN were used for modeling the geometry and determining the modes of each telescope. The objective was to have a first mode for the transmitter near 10 Hz, with the receiver being about slightly higher, due to less mass and the same stiffness.

This requirement was changed to around 1 Hz for the purposes of propagating an answer. Lower modal frequencies take less time to propagate.

a. PATRAN Telescope Geometry

	Transmitter	Receiver
Inner Diameter (m)	1.573	1.573
Outer Diameter (m)	2.360	2.360
Length (m)	4.000	4.000
Mass (kg)	2267.6	972.36
Density (kg/m^3)	233.23	100.01
Young's Modulus (Pa)	1.00E+08	1.00E+08
Poisson's Ratio	0.3	0.3

Figure 11 Flexible Body Parameters from Geometry in PATRAN

b. NASTRAN Normal Modes

The resultant modes from NASTRAN are shown in Figure 12. During simulation, the impacts of flexibility were impractical for such high frequencies. Therefore, the modes were modified with a flexibility factor. It was determined that reducing the modes by a factor of ten resulted in a manageable simulation. The modes used for simulation are shown in Figure 13.

Mode	Transmitter	Receiver
1	8.59	13.09
2	10.31	15.72
3	16.73	25.52
4	18.52	28.24
5	27.64	42.16
6	39.58	60.35
7	47.99	73.18
8	49.67	75.75
9	51.92	79.18
10	67.57	103.04

Figure 12 Receiver and Transmitter Modes from NASTRAN (Hz)

Mode	Transmitter	Receiver
1	0.86	1.31
2	1.03	1.57
3	1.67	2.55
4	1.85	2.82
5	2.76	4.22
6	3.96	6.04
7	4.80	7.32
8	4.97	7.58
9	5.19	7.92
10	6.76	10.30

Figure 13 Receiver and Transmitter Modes Used in Simulation (Hz)

c. Modeling Rigid-Elastic Coupling

The rigid-elastic coupling matrix was not taken from a finite element analysis program. Instead was chosen arbitrarily, from visual inspection of the displayed modes in the simulation mode of PATRAN. However, the method used could easily be substituted by NASTRAN output. The arbitrary method used involved selecting a unit vector for each mode considered, and then multiplying this by a coupling factor. The unit vectors represent the amount of the coupling that is occurring between an axis of rotation and a generalized coordinate. The first two modes are bending modes about the x and y-axis respectively. The third mode is a twisting mode about the z-axis. The fourth and fifth modes are combinations of these effects. The rigid-elastic coupling matrix was adjusted such that the maximum coupling occurred from the first mode, and the minimum coupling occurred from the last mode considered. The coupling factors varied from a maximum of 10% to a minimum of 1% of the maximum principal moment of inertia, and are shown in Figure 14.

Mode	Coupling Factor
1	7000
2	5425
3	3850
4	2275
5	700

Figure 14 Rigid-Elastic Coupling Factors for Simulation

The rigid-elastic coupling matrix is presented in the following, where $M_{AEO} = M_{\rho EO} = M_{\tau EO}$.

$$M_{AEO} = CouplingFactorMatrix * CouplingVectors$$

$$= \begin{bmatrix} 7000 & 0 & 0 & 0 & 0 \\ 0 & 5425 & 0 & 0 & 0 \\ 0 & 0 & 3850 & 0 & 0 \\ 0 & 0 & 0 & 2275 & 0 \\ 0 & 0 & 0 & 0 & 700 \end{bmatrix} \begin{bmatrix} 1 & 0 & 0 \\ 0 & 1 & 0 \\ 0 & 0 & 1 \\ 0.7071 & 0 & 0.7071 \\ 0.7071 & 0.7071 & 0 \end{bmatrix}$$

$$= \begin{bmatrix} 7000 & 0 & 0 \\ 0 & 5425 & 0 \\ 0 & 0 & 3850 \\ 1608.67 & 0 & 1608.67 \\ 494.975 & 494.975 & 0 \end{bmatrix} kg - m^2$$

2. Observing System Free-Free Behavior

Nominally, all generalized coordinates are assigned an initial condition of zero. In order to demonstrate the uncontrolled dynamics, generalized coordinates are given random initial conditions, and no actuation is applied. The telescope joint angle motion and spacecraft attitude actuators (reaction wheels) are set to zero input. This is equivalent to stretching and compressing various springs in an undamped multi-body spring-mass system and letting them go. The purpose is to observe the free-free behavior of the system.

Figure 15 was created with random initial conditions for the generalized coordinates. Additionally, the initial angular rate of the transmitter was [0,0,0] rad/sec. There was no commanded angular acceleration of the transmitter or receiver, and there was no initial angular momentum. The purpose of this figure is to demonstrate the complex frequency content of the response. The order of magnitude of the difference in angular rates is not to be compared to future graphs. Since the initial conditions are random, any such comparison would be meaningless.

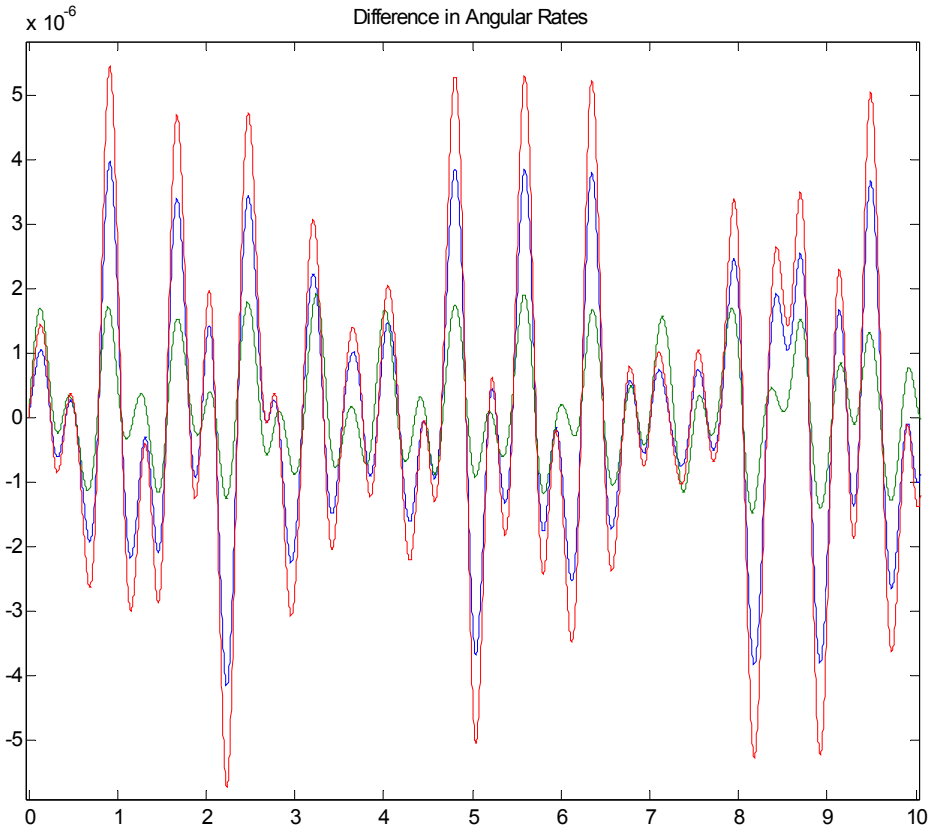

Figure 15 Uncommanded Free-Free Behavior, Angular Rates

3. Eigenvalues of the Free-Free System

Fundamentally, the free-free behavior of the system is dependent on the joint angle. This assumes that the rate of motion has no effects on the free-free modal behavior. Since the input has no effect on the modes, the base equation is shown in.

Equation 24: Free-Free Dynamics, No External Forces

$$\begin{bmatrix} I & 0 & M_{AEO} \\ 0 & I & M_{AEO} \\ M_{AEO}{}^T & M_{AEO}{}^T & M_{ARO} \end{bmatrix} \begin{Bmatrix} \ddot{q}_\tau \\ \ddot{q}_\rho \\ \ddot{U} \end{Bmatrix} \begin{bmatrix} \omega_\tau{}^2 & 0 & 0 \\ 0 & \omega_\rho{}^2 & 0 \\ 0 & 0 & 0 \end{bmatrix} \begin{Bmatrix} q_\tau \\ q_\rho \\ U \end{Bmatrix} = \begin{Bmatrix} 0 \\ 0 \\ 0 \end{Bmatrix}$$

When this is put into the eigenvalue format, we have Equation 25.

Equation 25: Free-Free Dynamics, Eigenvalue Solution

$$\det\left\{\lambda^2 I - M^{-1}K\right\} = 0$$

where

$$M = \begin{bmatrix} I & 0 & M_{AEO} \\ 0 & I & M_{AEO} \\ M_{AEO}{}^T & M_{AEO}{}^T & M_{ARO} \end{bmatrix}$$

$$K = \begin{bmatrix} \omega_\tau{}^2 & 0 & 0 \\ 0 & \omega_\rho{}^2 & 0 \\ 0 & 0 & 0 \end{bmatrix}$$

A simulation was created to determine the eigenvalues of the system at a family of joint angles $\alpha \in [0 \quad \pi]$. This simulation solves Equation 25, and is shown in Figure 16.

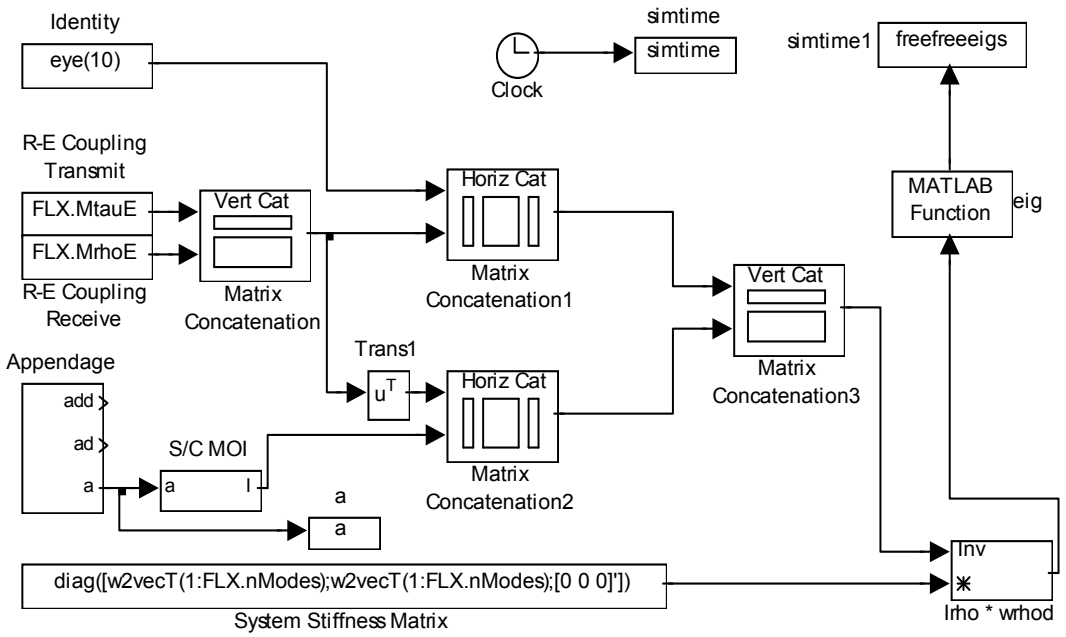

Figure 16 SIMULINK Model for Determining Eigenvalues of the Free-Free System, using Equation 25

The eigenvalues are sensitive to the coupling factors for the rigid-elastic coupling. As the coupling factors are reduced, the system free-free frequencies approach the modes of each single body. These free-free modes are what must

be compensated for in the control system. For the coupling factors used, the free-free system frequencies are shown in Figure 17. The column identified as "without coupling" uses coupling factors of zero. In all columns, the rigid body modes are omitted, as the frequencies are zero for these modes.

Frequencies (rad/sec)		
with coupling	without coupling	List of Single Body Modes
0	5.3949	5.3949
0	6.4756	6.4756
0	8.2272	8.2272
6.947	9.8752	9.8752
8.349	10.5144	10.5144
11.374	11.637	11.637
13.737	16.0343	16.0343
17.299	17.3696	17.3696
17.426	17.7463	17.7463
26.411	26.4884	26.4884

Figure 17 Free-Free Modes with and without Rigid-Elastic Coupling

D. SENSITIVITY OF PLANT BEHAVIOR TO UNCOMPENSATED PD CONTROLLER BANDWIDTH

This section shows the interaction between the PD controller bandwidth and the flexible plant, without any compensator applied. This is accomplished by turning off all compensators in the model, holding the time constant unchanged, and steadily increasing the controller gain.

Fundamentally, designing a control law for a system with flexible bodies seeks high bandwidth control to achieve fine pointing, while not exciting flexible modes. When the original rigid body gains for the PD controller were applied to the flexible system, they were too low. The attitude and rate errors which occurred were due to a low controller gain, and not vibration. To achieve higher pointing accuracy, the controller gains were increased while the time constants were unchanged.

The original rigid body controller had gains around 5000 and time constant around 0.3 sec. The time constant was adjusted to $\tau = 0.01\,\text{sec}$ in order to lower the damping of the rigid body controller. Then, the gains were adjusted to find

the points of instability for various modes. The highest stable gain was determined, as well as the gain which caused instability for the first three modes. The adjusted values of K increase the bandwidth of the controller, and demonstrate structure-controls interaction.

The figures that follow show the results of the uncompensated flexible body for increasing gains. There are three plots in each figure. The top plot is the difference in quaternions. This has no physical meaning, but does allow the user to see the rate at which error is occurring. The middle plot is the difference in angular rates: commanded rate minus actual rate. The bottom plot is the pointing error, in radians: angle subtended between the actual attitude and the commanded attitude.

In Figure 21, the angular rate errors are on the order of 1e-6 rad/sec, and the pointing error continues to grow. This is an effect of a low gain. In Figure 22, Figure 23 and Figure 24, the angular rate errors continue to decrease, and the onset of angular error is delayed. Finally, in Figure 25 there is no angular error throughout the simulation. Now the gain is increased until the plant cannot be controlled. The rate error continues to decrease in Figure 26 and Figure 27. However, in Figure 28, the system instability is obvious.

Through trial and error, the gains at which each axis want unstable were determined. Figure 29 shows the behavior at the highest stable gain, 50.3e6. At this gain, the angular rate error is on the order of 5e-10 rad/sec. Uncompensated gains above this level result in rate errors on the order of 5e-4 rad/sec, one million times higher than the highest stable gain. The first instability occurs at 50.4e6, as shown in Figure 30. The second axis is unstable at 85.7e6, as shown in Figure 31. The third axis is unstable at 93.6e6, as shown in Figure 32. For all of these simulations, the initial pointing error was 10 nanoradians. That causes the initial oscillation.

Gain	Max Rate Error at 20 seconds (rad/sec)	Angle Error at 20 seconds (rad)
5,000.00	5.E-06	3.E-05
20,000.00	1.E-06	8.E-06
80,000.00	3.E-07	2.E-06
320,000.00	1.E-07	3.E-07
1,280,000.00	2.E-08	0
5,120,000.00	5.E-09	0
20,480,000.00	1.E-09	0
50,300,000.00	5.E-10	0
50,400,000.00	5.E-04	4.E-04
93,600,000.00	7.E-04	6.E-04

Figure 18 PD Controller Gain and Corresponding Errors for Flexible Spacecraft, Without Compensator

Gain	Compensator Type	Omega_z	Omega_p	Zeta_z	Zeta_p	Max Rate Error at 20 seconds (rad/sec)	Angle Error at 20 seconds (rad)
51,000,000	NMP Notch	first three modes		-0.00001	1	5.00E-08	0
60,000,000	NMP Notch	first three modes		-0.00001	0.7	4.00E-07	0
55,000,000	NMP Notch	first three modes		-0.00001	0.7	3.00E-07	0

Figure 19 PD Controller Gain and Corresponding Errors for Flexible Spacecraft, Nonminimum Phase Notch Filter

Gain	Compensator Type	Omega_z	Omega_p	Zeta_z	Zeta_p	Max Rate Error at 20 seconds (rad/sec)	Angle Error at 20 seconds (rad)
51,000,000	Phase Lag	14	6	1	1.5	5.00E-10	0
60,000,000	Phase Lag	14	6	1	1.5	4.00E-10	0
86,000,000	Phase Lag	14	6	1	1.5	3.00E-10	0
95,000,000	Phase Lag	14	6	1	1.5	3.00E-10	0
105,000,000	Phase Lag	14	6	1	1.5	3.00E-10	0
115,000,000	Phase Lag	14	6	1	1.5	2.00E-10	0
125,000,000	Phase Lag	14	6	1	1.5	2.00E-10	0
140,000,000	Phase Lag	14	6	1	1.5	1.80E-10	0
160,000,000	Phase Lag	14	6	1	1.5	1.50E-10	0
258,000,000	Phase Lag	14	6	1	1.5	1.00E-10	0
258,000,000	Phase Lag	20	6	0.3	0.33	1.20E-10	0
258,000,000	Phase Lag	20	6	0.3	0.35	1.20E-10	0
258,000,000	Phase Lag	20	6	0.2	0.21	1.20E-10	0
500,000,000	Phase Lag	20	6	0.2	0.21	5.00E-11	0

Figure 20 PD Controller Gain and Corresponding Errors for Flexible Spacecraft, Phase Lag Filter

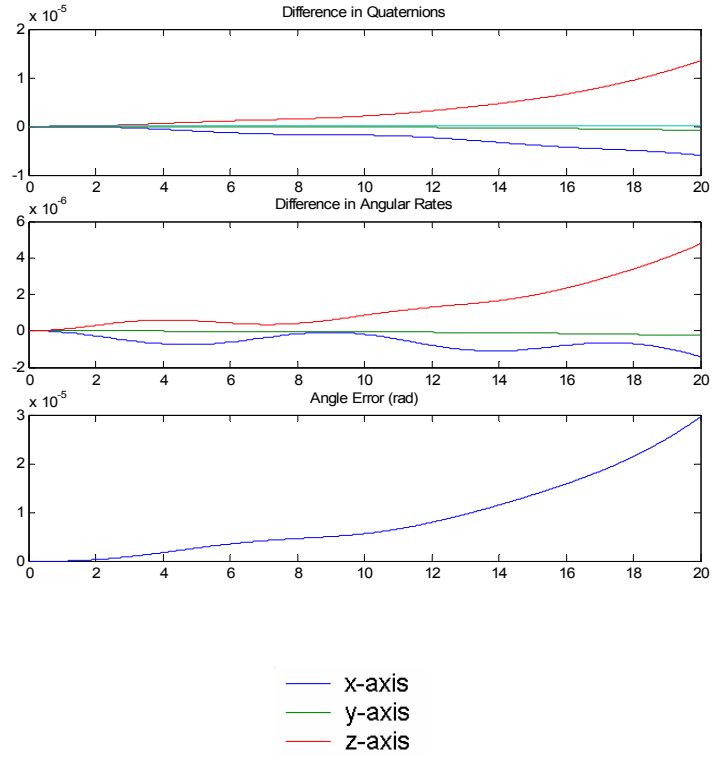

Figure 21 Uncompensated Behavior, K = 5000

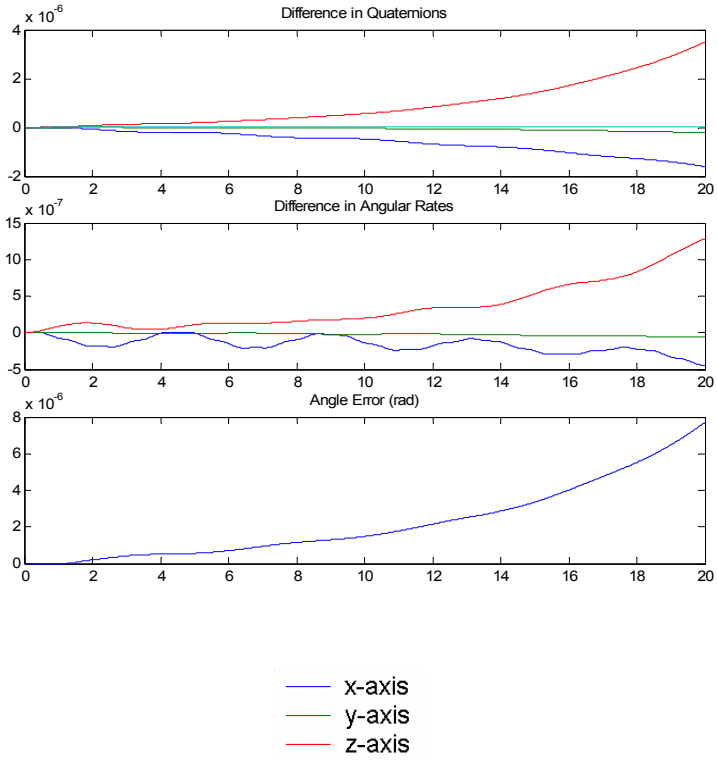

Figure 22 Uncompensated Behavior, K = 20,000

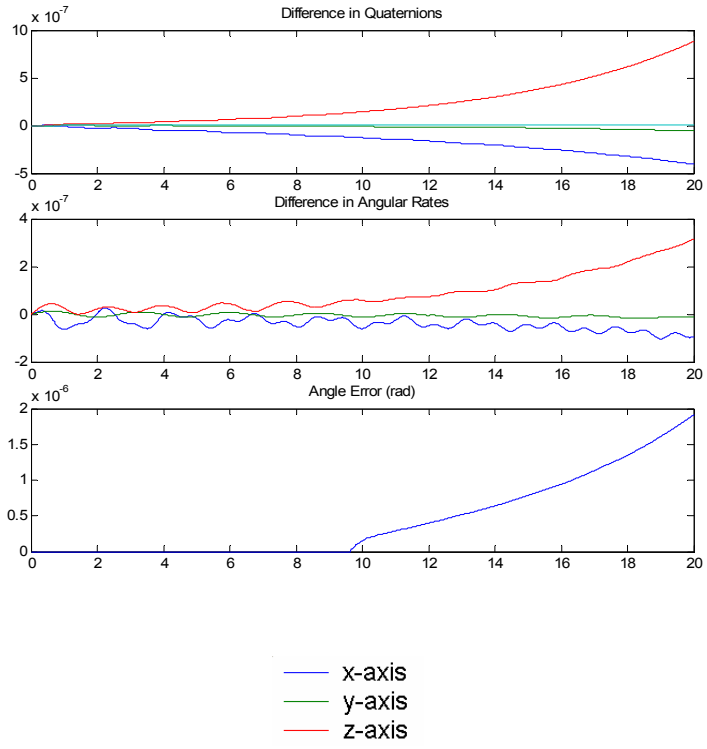

Figure 23 Uncompensated Behavior, K = 80,000

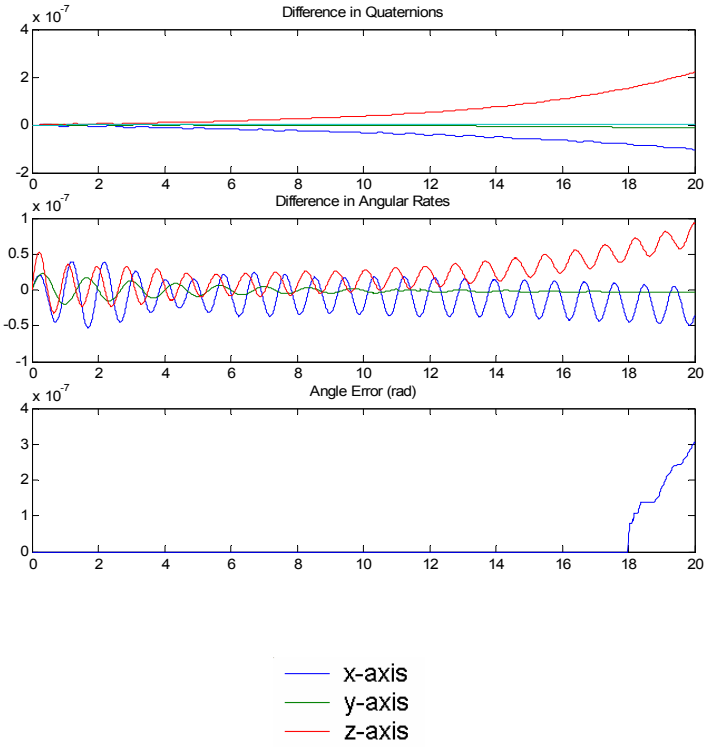

Figure 24 Uncompensated Behavior, K = 320,000

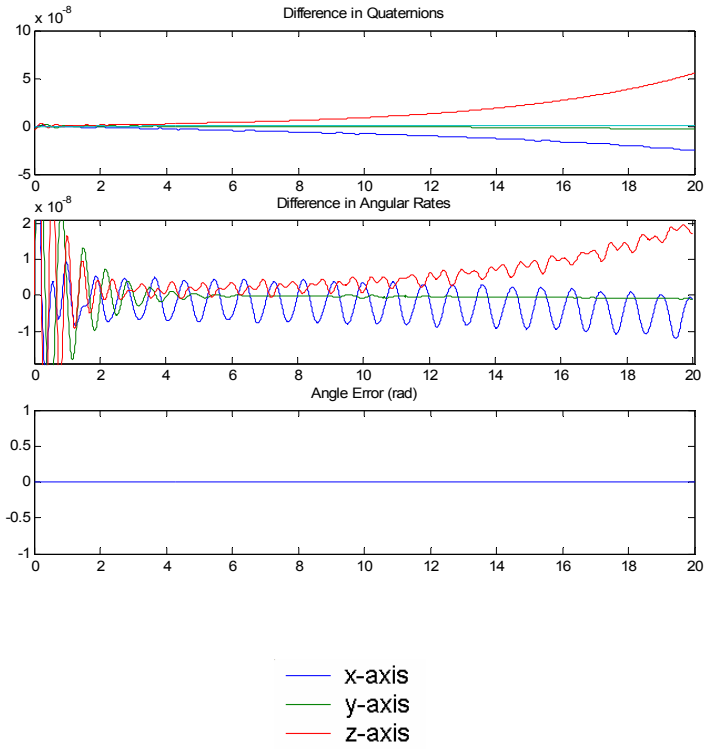

Figure 25 Uncompensated Behavior, K = 1,280,000

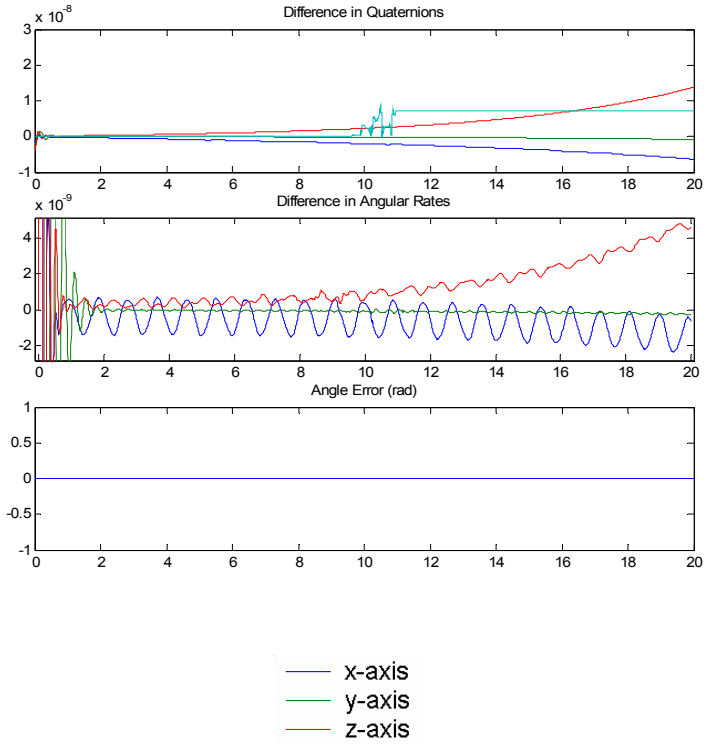

Figure 26 Uncompensated Behavior, K = 5,120,000

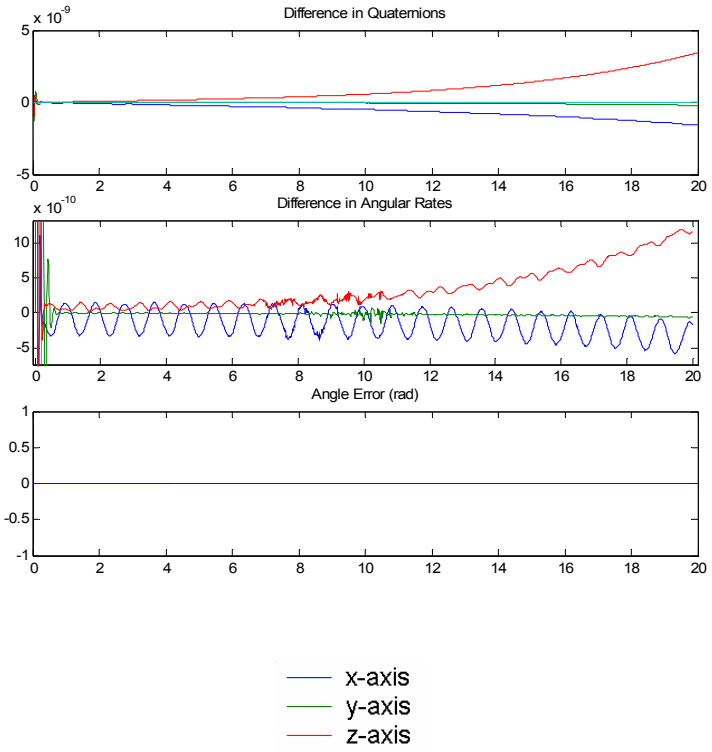

Figure 27 Uncompensated Behavior, K = 20,480,000

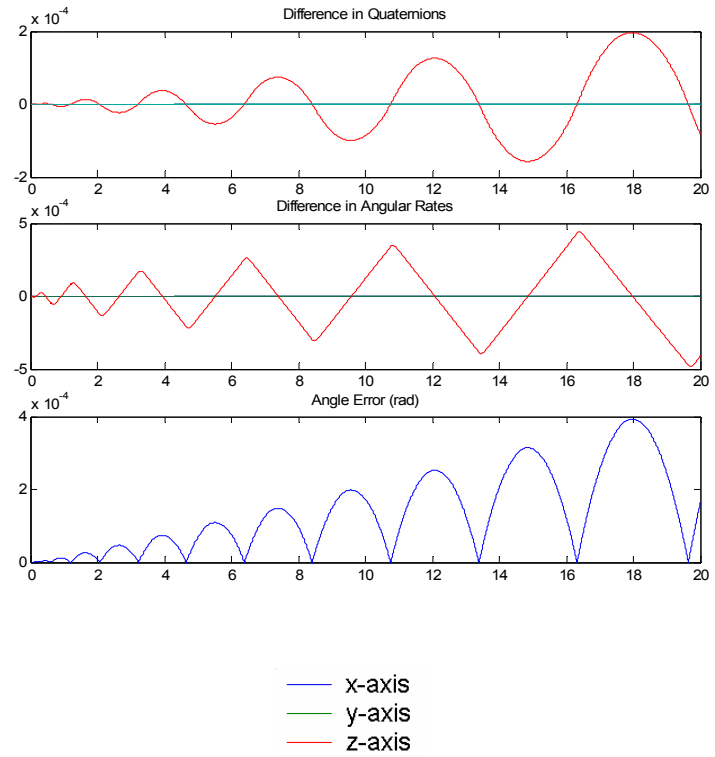

Figure 28 Uncompensated Behavior, K = 81,920,000

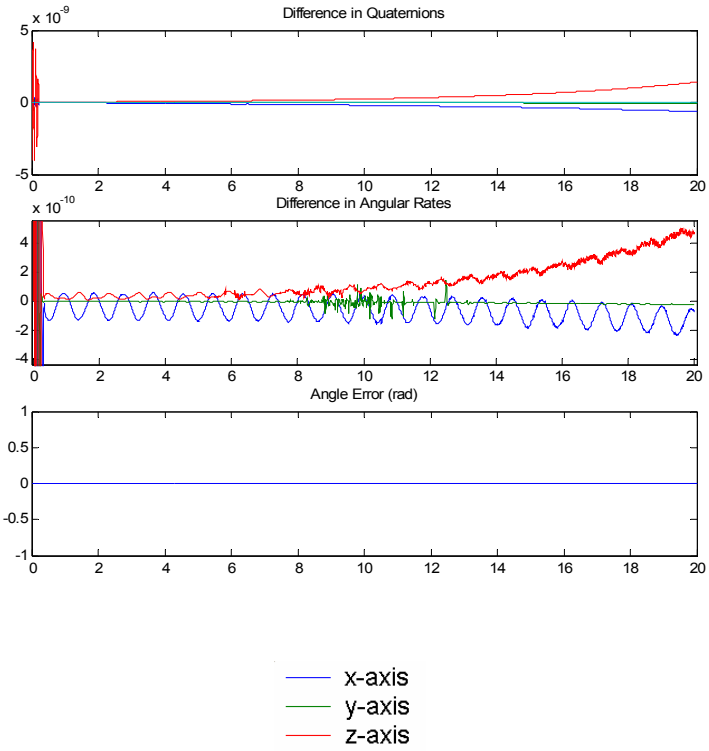

Figure 29 Uncompensated Behavior, K = 50,300,000, the last stable gain

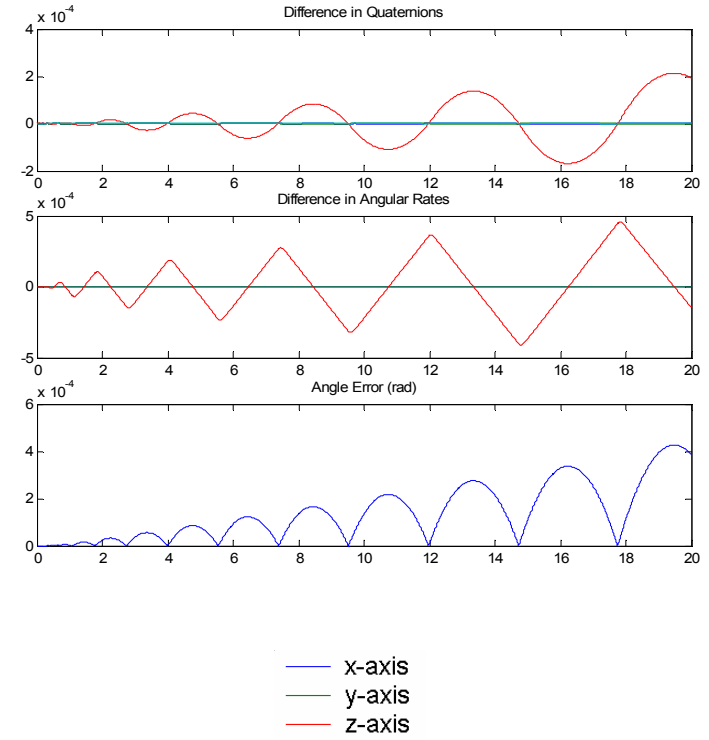

Figure 30 Uncompensated Behavior, K = 50,400,000, two axes unstable

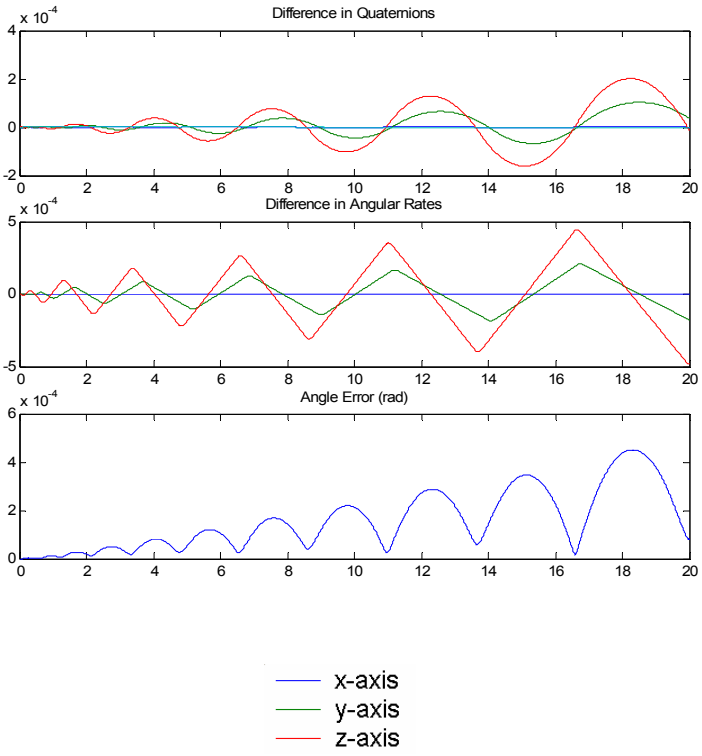

Figure 31 Uncompensated Behavior, K = 85,700,000, onset of second axis unstable

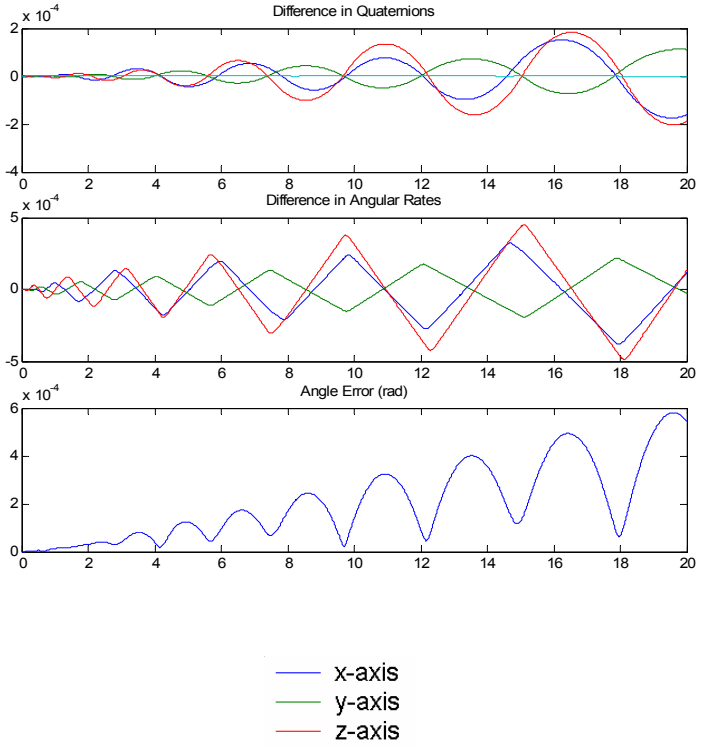

Figure 32 Uncompensated Behavior, K = 93,600,000, onset of third axis unstable

VI. COMPENSATOR APPLICATION TO ANALYTICAL MODEL

Based on the compensators described in Chapter IV, two applicable designs were selected for application to this control system. The Nonminimum-Phase Notch Filter and the Minimum-Phase Lag Filter were chosen for this undamped system. The conventional Minimum Phase Notch Filter is not applicable since there is no passive system damping for the flexible modes. The structural filters used in industry are of the Minimum-Phase Lead variant. This type of filter was attempted. However, no performance increases were realized. The lowest error achieved without a compensator occurred at K = 50.3e6. At this gain, the angle error is numerically “zero”. Although, it is not zero, it is below the threshold of which MATLAB is able to take the arccosine. The rate error at the end of the simulation was approximately 5e-10 rad/sec. The objective of the compensator is to reduce this rate error, thereby reducing the impact of structural vibrations on the pointing error budget.

A. NONMINIMUM PHASE NOTCH FILTER

The first method used was the nonminimum phase notch filter. The compensators were designed about each identified free-free frequency. Initially, one was applied. By the end, three compensators were applied, with the purpose of suppressing the first three modes. The best performance achieved was on the order of 3e-8 rad/sec. Unfortunately, this is worse than the uncompensated system before the onset of instability. The results are shown below.

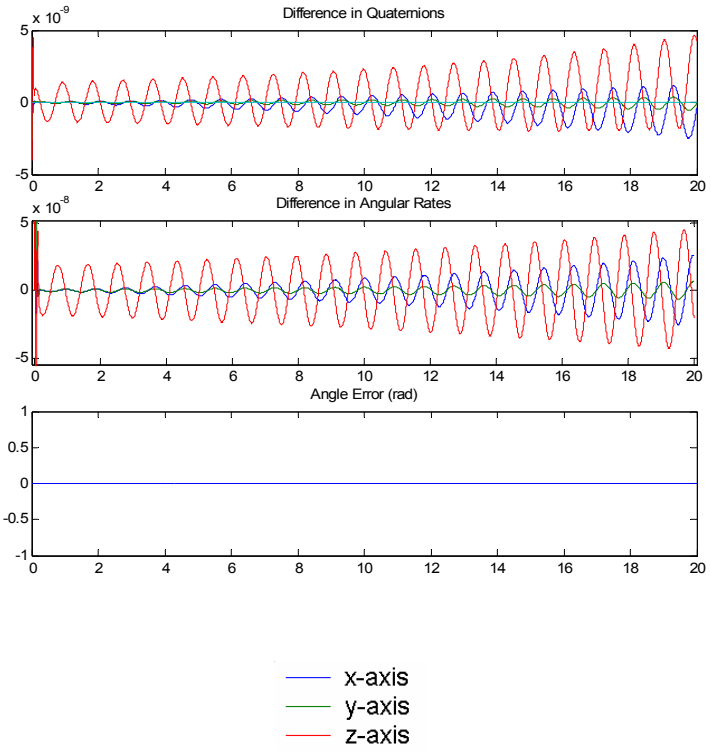

Figure 33 Notch Filter, K = 51e6, $\zeta_Z = -0.00001$, $\zeta_P = 1.0$

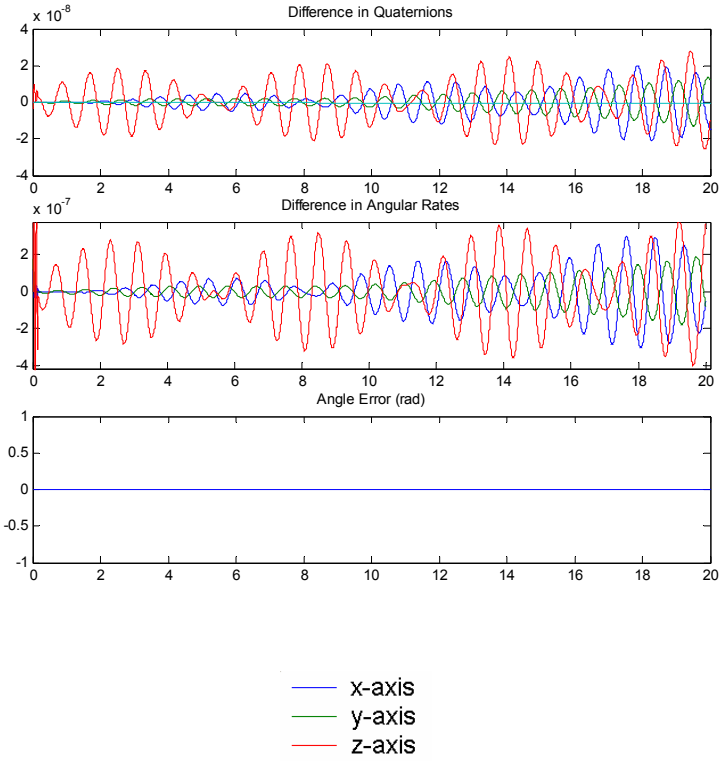

Figure 34 Notch Filter, K = 60e6, $\zeta_Z = -0.00001$, $\zeta_P = 0.7$

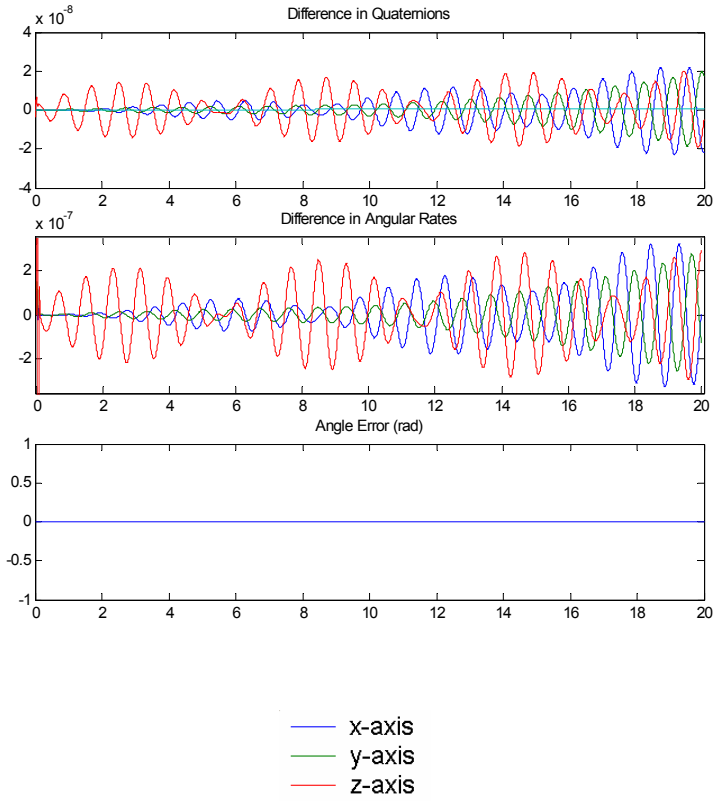

Figure 35 Notch Filter, K = 55e6, $\zeta_Z = -0.00001$, $\zeta_P = 0.7$

B. MINIMUM PHASE LAG FILTER

The second method used was the minimum phase notch filter. The compensators were designed about the identified free-free frequency. The best performance achieved was on the order of 5e-11 rad/sec. This is a factor of ten reduction in angular rate error.

Initially, a highly damped filter was used. With ζ_Z=1 and ζ_P=1.5 , the gain was steadily increased from Figure 36 through Figure 45. The rate error in Figure 45 was reduced to 1e-10 rad/sec. At this point, with a gain of 258e6, the error has been reduced by a factor of five.

After this, the filter was lightly damped. The zeros had damping ratios between 0.2 and 0.3. The poles had damping ratios 1.05 times that of the zeros. Different cases are presented in Figure 46 through Figure 49. The rate error in

Figure 49 was reduced to 5e-11 rad/sec. At this point, with a gain of 500e6, the error has been reduced by a factor of ten.

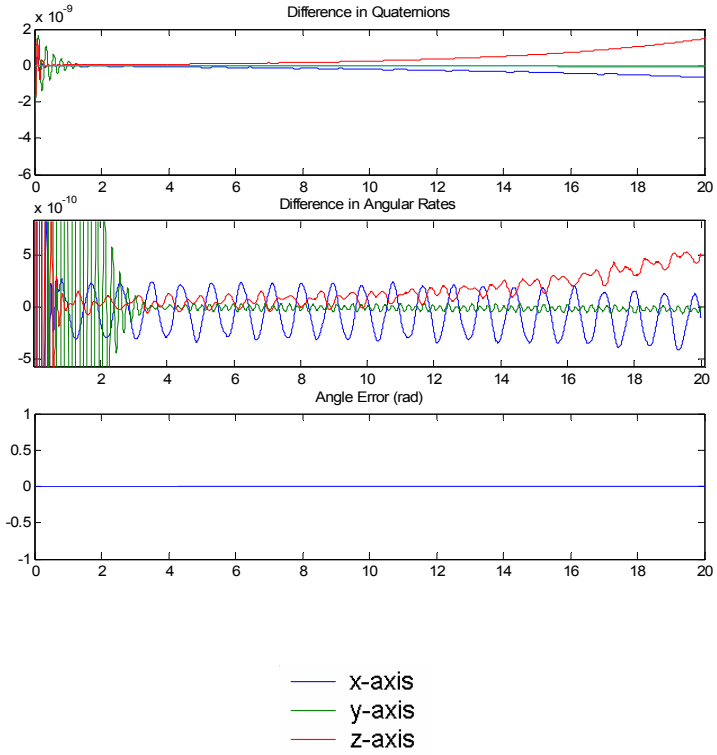

Figure 36 Phase Lag Filter, K=51e6, ζ_Z=1, ζ_P=1.5, ω_Z=14, ω_P=6

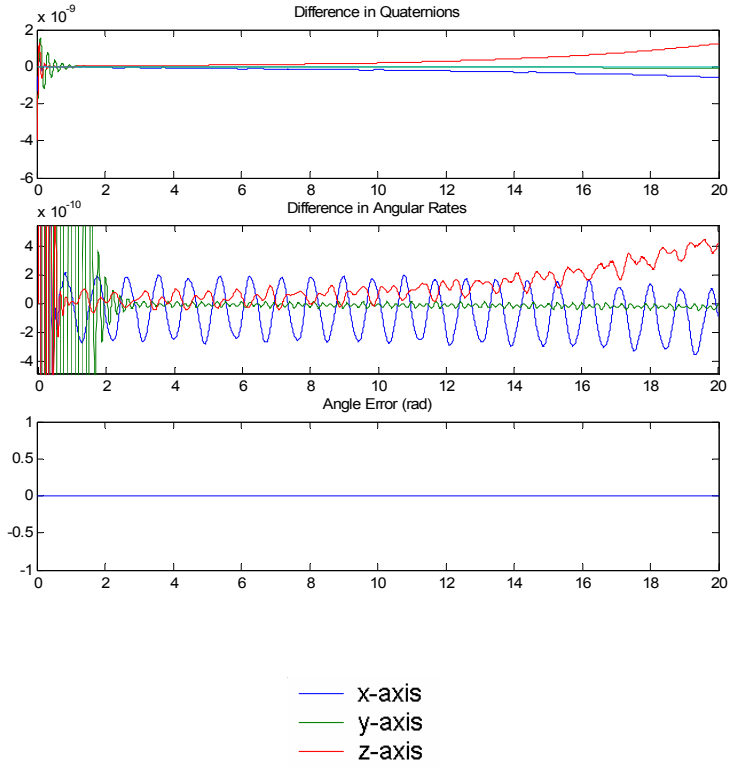

Figure 37 Phase Lag Filter, K=60e6, ζ_Z=1, ζ_P=1.5, ω_Z=14, ω_P=6

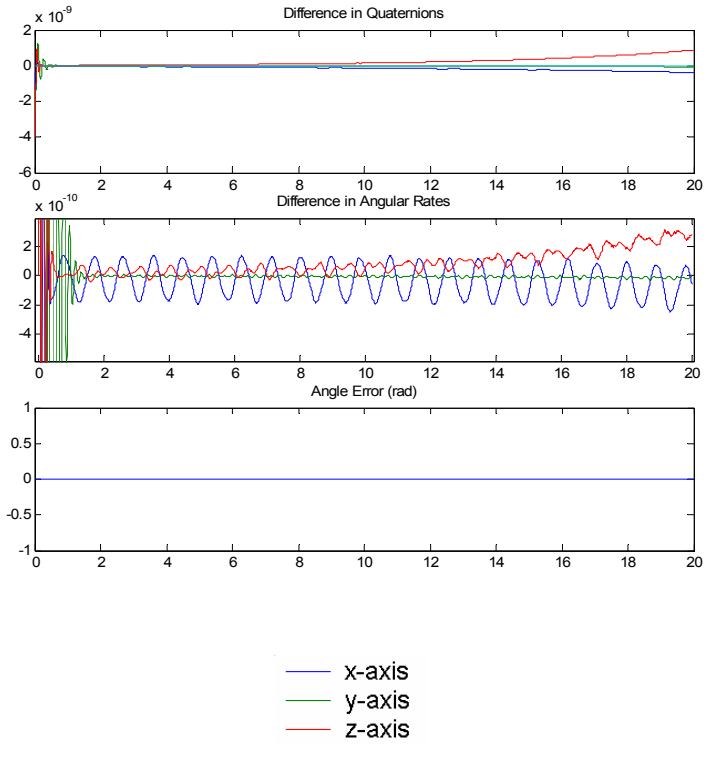

Figure 38 Phase Lag Filter, K=86e6, ζ_Z=1, ζ_P=1.5, ω_Z=14, ω_P=6

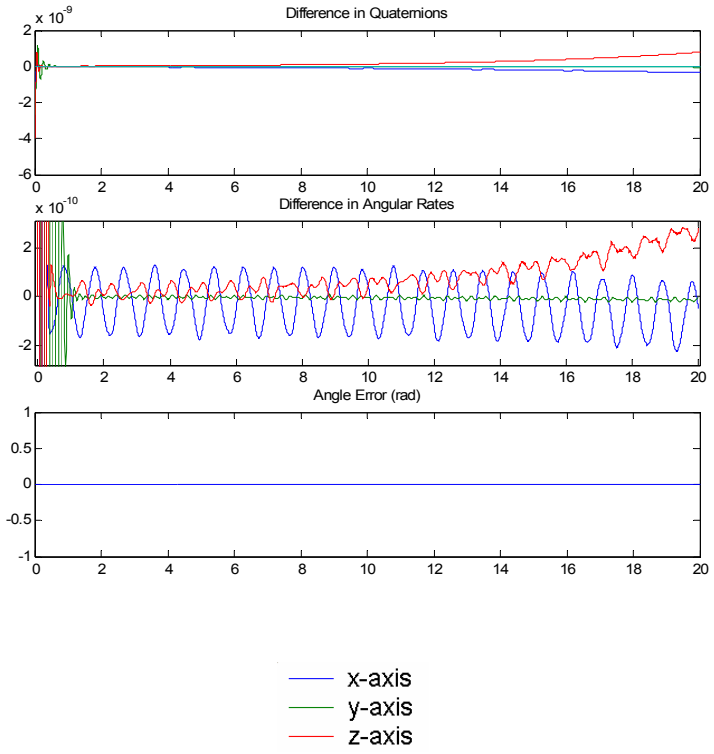

Figure 39 Phase Lag Filter, K=95e6, ζ_Z=1, ζ_P=1.5, ω_Z=14, ω_P=6

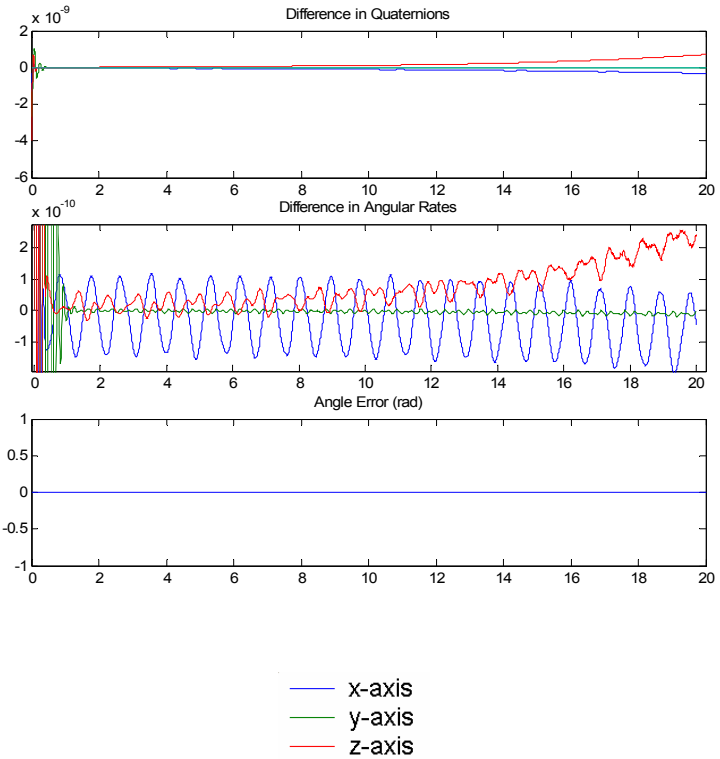

Figure 40 Phase Lag Filter, K=105e6, ζ_Z=1, ζ_P=1.5, ω_Z=14, ω_P=6

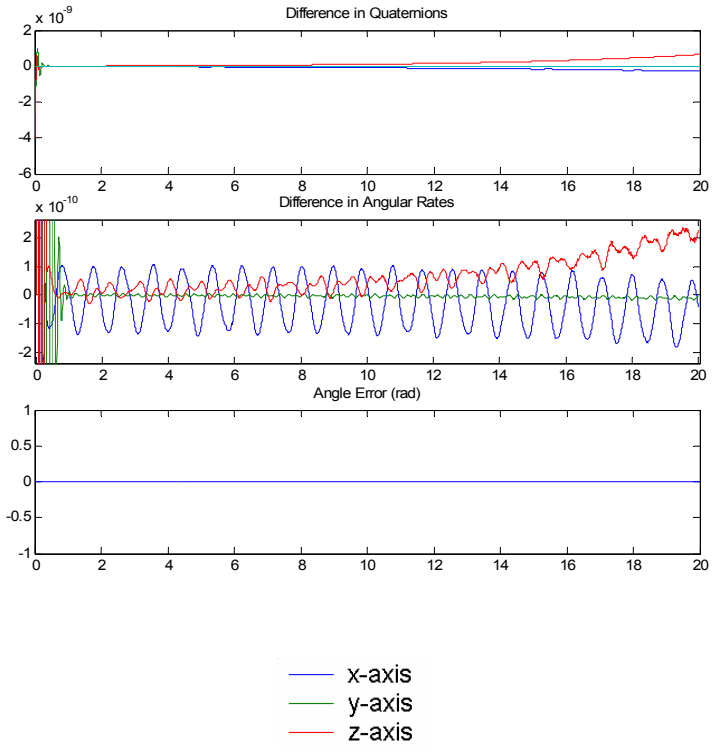

Figure 41 Phase Lag Filter, K=115e6, ζ_Z=1, ζ_P=1.5, ω_Z=14, ω_P=6

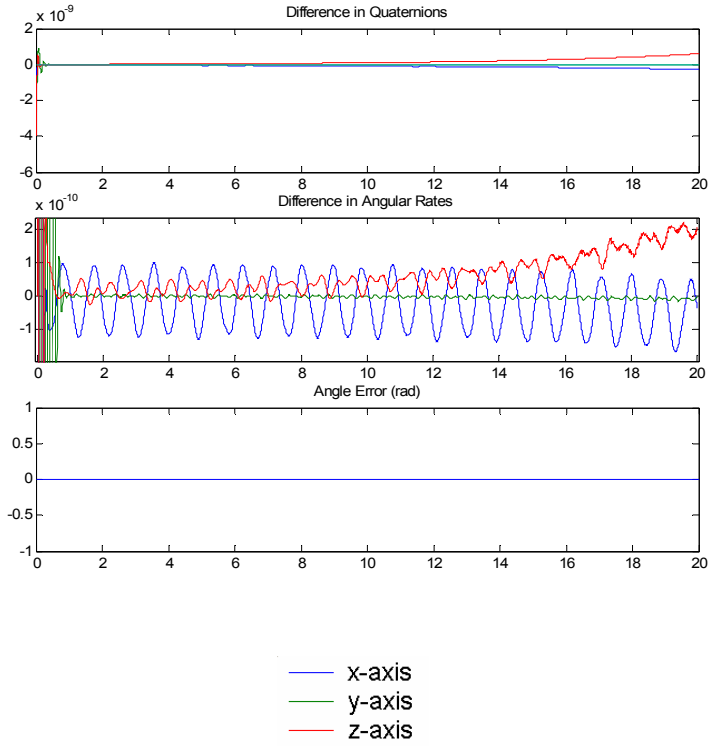

Figure 42 Phase Lag Filter, K=125e6, ζ_Z=1, ζ_P=1.5, ω_Z=14, ω_P=6

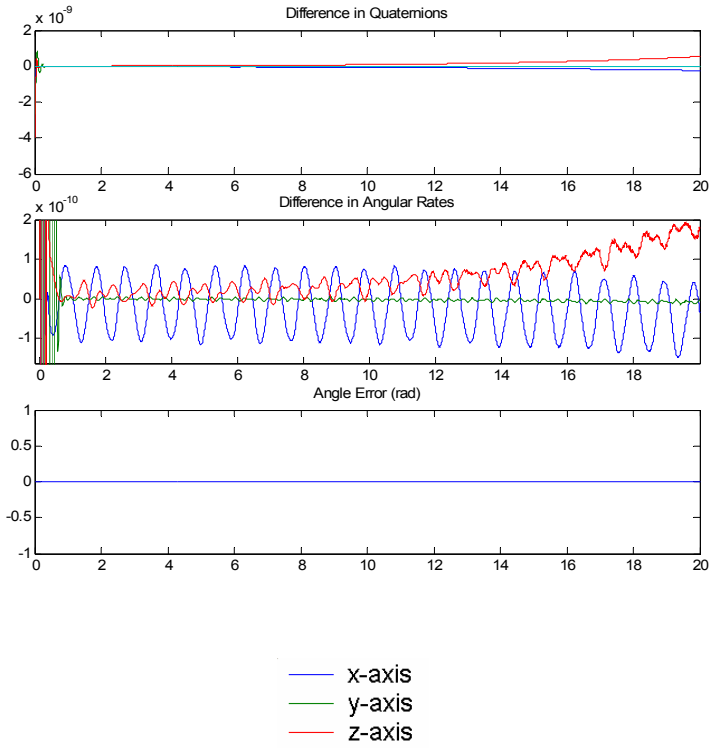

Figure 43 Phase Lag Filter, K=140e6, ζ_Z=1, ζ_P=1.5, ω_Z=14, ω_P=6

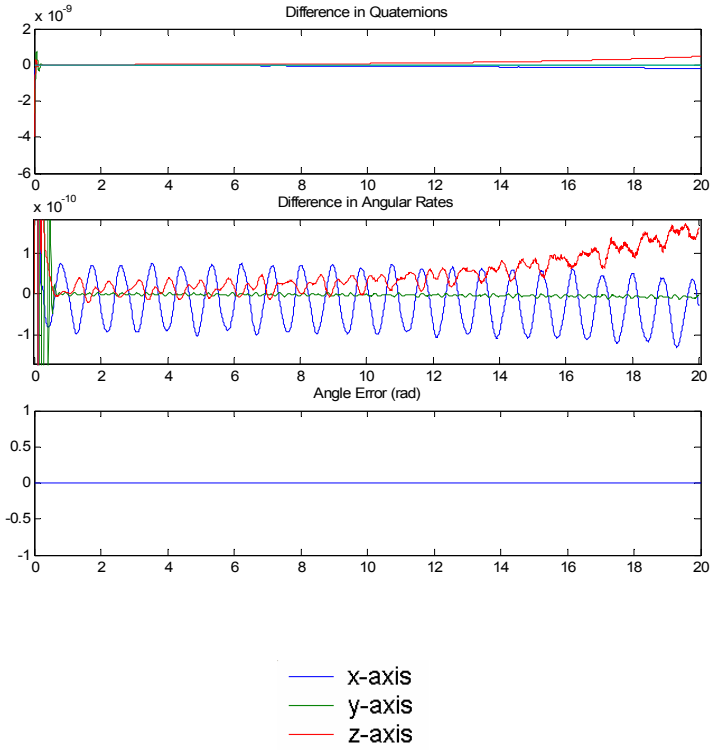

Figure 44 Phase Lag Filter, K=160e6, ζ_Z=1, ζ_P=1.5, ω_Z=14, ω_P=6

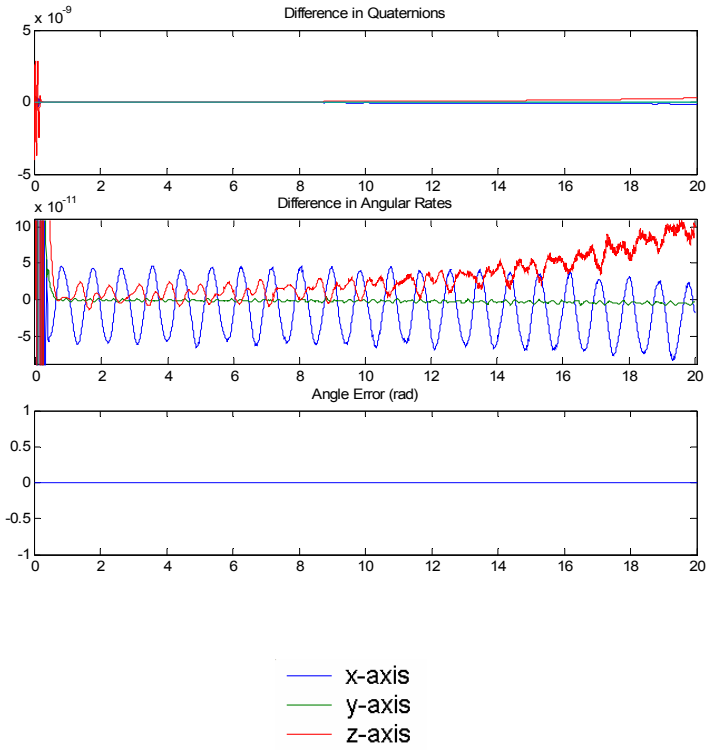

Figure 45 Phase Lag Filter, K=258e6, ζ_Z=1, ζ_P=1.5, ω_Z=14, ω_P=6

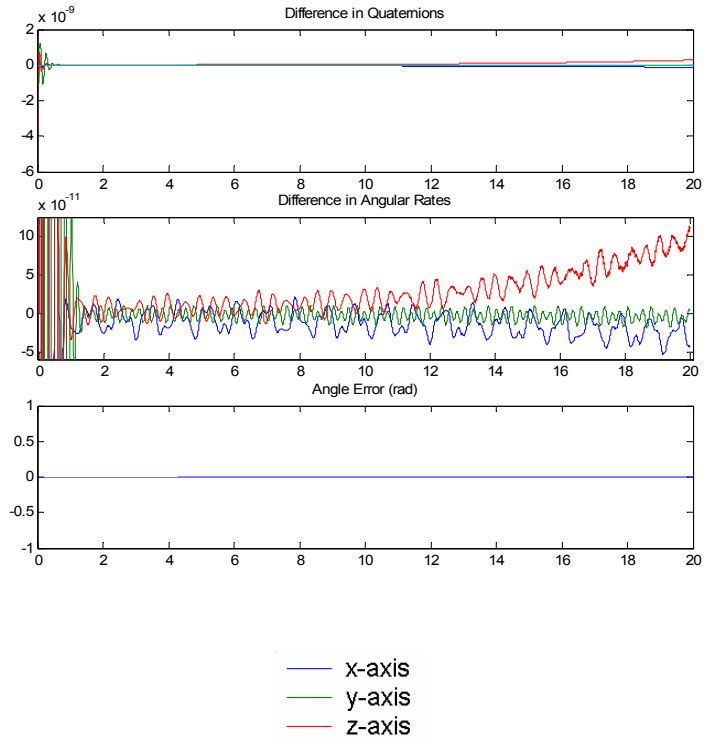

Figure 46 Phase Lag Filter, K=258e6, ζ_Z=0.3, ζ_P=0.33, ω_Z=20, ω_P=6

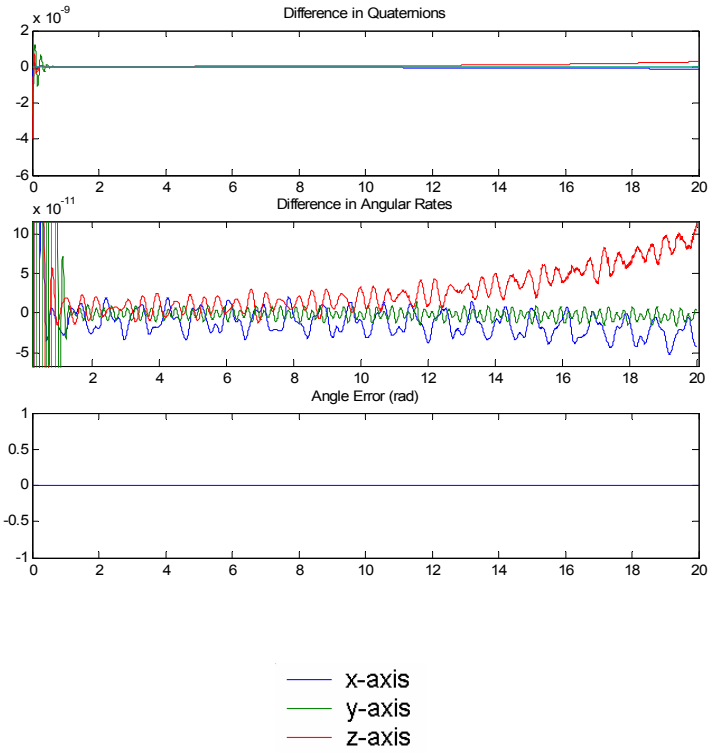

Figure 47 Phase Lag Filter, K=258e6, ζ_Z=0.33, ζ_P=0.35, ω_Z=20, ω_P=6

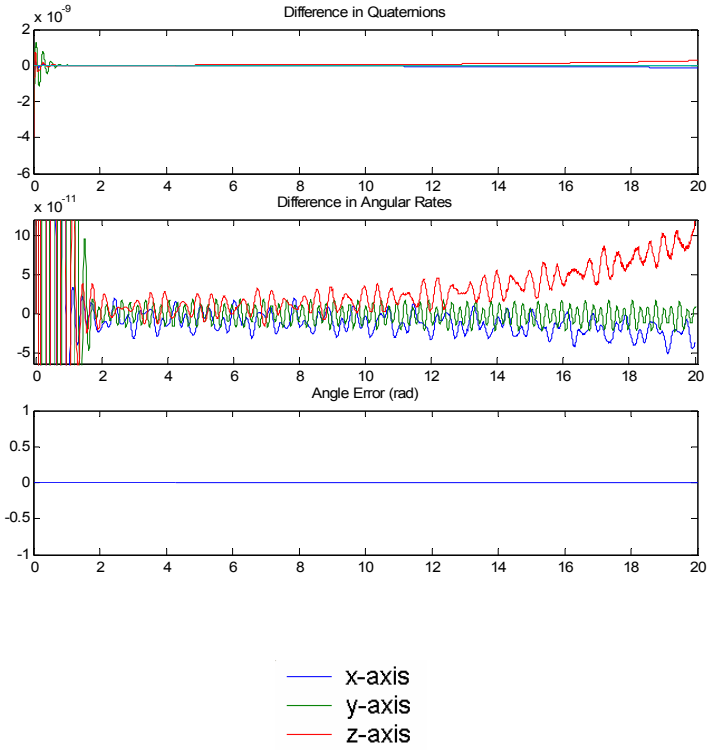

Figure 48 Phase Lag Filter, K=258e6, ζ_Z=0.2, ζ_P=0.21, ω_Z=20, ω_P=6

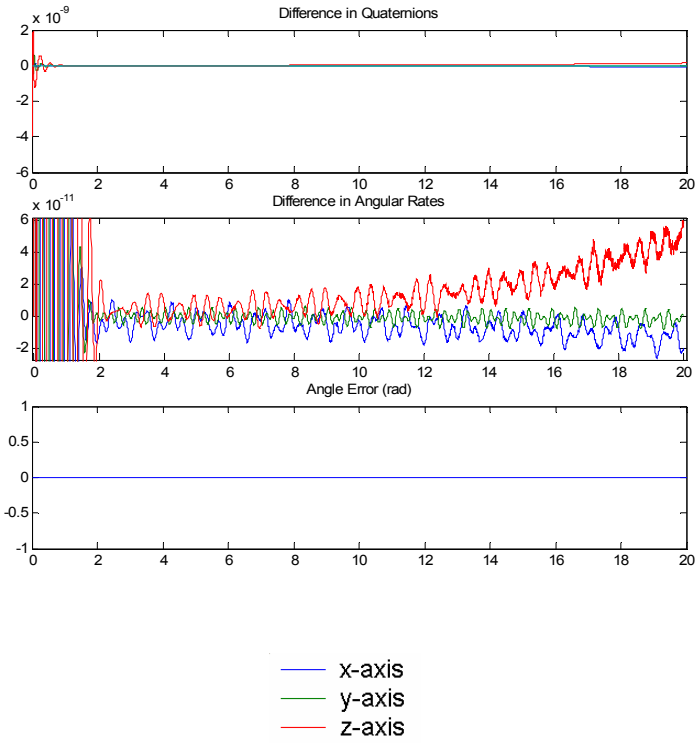

Figure 49 Phase Lag Filter, K=500e6, ζ_Z=0.2, ζ_P=0.21, ω_Z=20, ω_P=6

THIS PAGE INTENTIONALLY LEFT BLANK

VII. CONCLUSION

The design requirements for the Bifocal Relay Mirror spacecraft include controlling jitter at the nanoradian level. Typically, tight pointing requirements require high structural stiffness, at the cost of increasing the on-orbit mass. To accomplish this, while minimizing the mass of the spacecraft, the structure will have some inherent flexibility. These flexible modes will interact with the pointing control, hence affecting the payload performance. The compensator design conducted in this thesis achieved order of magnitude improvements in controlling the rate error, hence jitter. This thesis presented the rigid body and flexible body dynamics, and compares the uncompensated and compensated performance of the spacecraft using a flexible plant. Classical compensator designs were reviewed and applied.

The plant in this work was nonlinear. No attempts were made to linearize the plant about a set of conditions, or for a given set of command inputs. The instabilities were found completely by trial and error. One alternate approach for determining the destabilizing gain would be to command a rotation about one of the principal axis. Even with a time variant parameter, this would provide a linear plant. This would allow the control designer to use classical controller design, such as root locus techniques, to determine the unstable gains. This thesis did no such linearization, as a primary task was to establish a baseline nonlinear simulation to which others could be compared.

This thesis showed that classical, high gain PD controllers are appropriate for rigid body control. However, when the controlled plant includes flexible modes, uncompensated high gain PD control causes extreme deviation due to unmodeled dynamics. The compensators used in this formulation validate their application on flexible spacecraft with high pointing accuracy, such as the Bifocal Relay Mirror. The relative motion of the two telescopes is slow in this case. No effort was made to adjust the compensator based on the joint angle motion

characteristics. Classical compensator synthesis was a sufficiently accurate method for controlling the feedback torque due to flexibility.

Through classical second-order compensators, the angular rate error was decreased by a factor of ten. Nonminimum phase notch filters and phase lag filters were used. Ultimately, the phase lag filters provided the best performance.

LIST OF REFERENCES

Brij N. Agrawal, Design of Geosynchronous Spacecraft, 1986

Bong Wie, Space Vehicle Dynamics and Control, 1998

THIS PAGE INTENTIONALLY LEFT BLANK

INITIAL DISTRIBUTION LIST

1. Defense Technical Information Center
   Ft. Belvoir, Virginia

2. Dudley Knox Library
   Naval Postgraduate School
   Monterey, California